iScience

CellPress
OPEN ACCESS

Article

Underwater instant adhesion mechanism of self-assembled amphiphilic hemostatic granular hydrogel from *Andrias davidianus* skin secretion

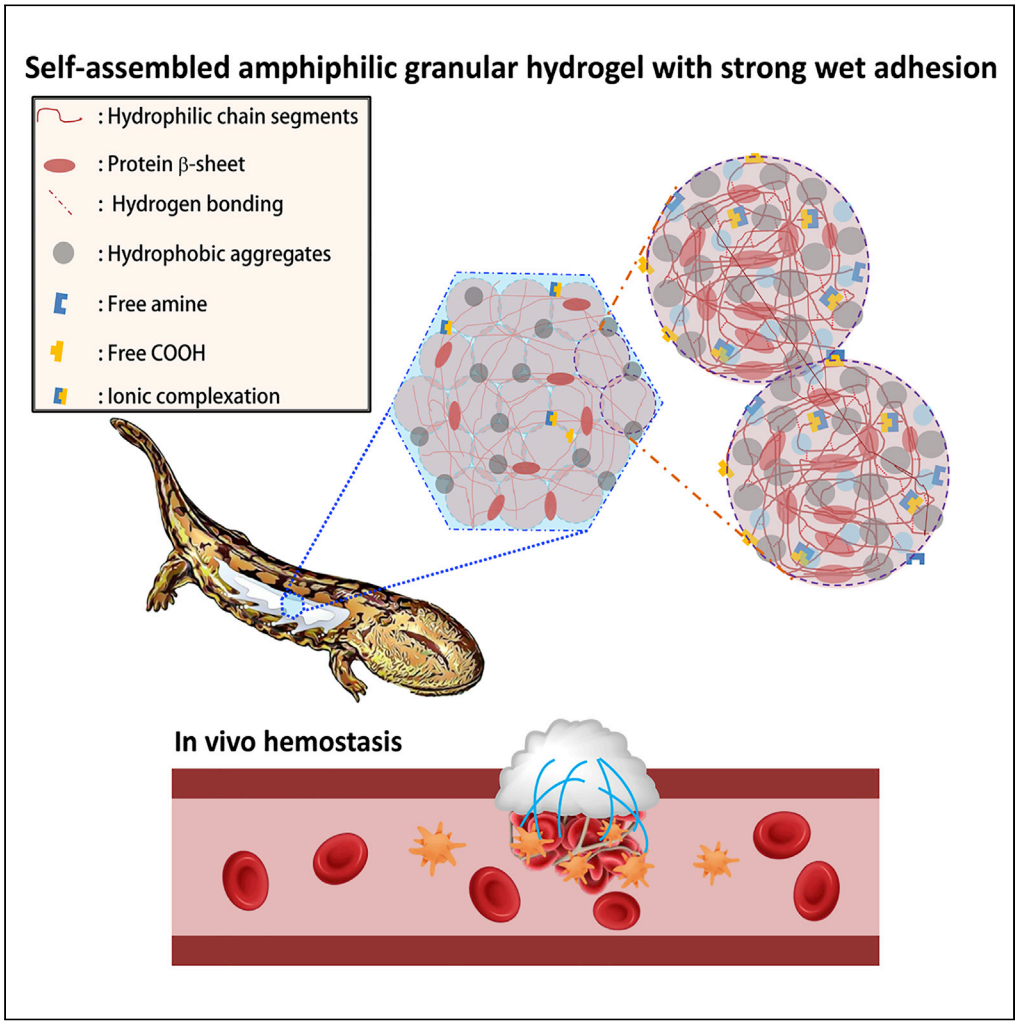

Yuqing Liu, Yinghao Li, Haitao Shang, ..., Chuhong Zhu, Malcolm Xing, Hong Wei

zhuch99@tmmu.edu.cn (C.Z.)
malcolm.xing@umanitoba.ca (M.X.)
weihong63@mail.sysu.edu.cn (H.W.)

Highlights

Dry granule adhesive of *Andrias davidianus* skin secretion build strong wet adhesion

The granules absorb water and self-assemble to form a hydrophobic adhesive in seconds

The adhesive showed 72-h underwater adhesion strength of ~47kPa on porcine skin tissue

Remarkable hemostasis effect was found on rat hepatic and cardiac hemorrhage model

Liu et al., iScience *25*, 105106
October 21, 2022
https://doi.org/10.1016/j.isci.2022.105106

iScience

CellPress
OPEN ACCESS

Article

Underwater instant adhesion mechanism of self-assembled amphiphilic hemostatic granular hydrogel from *Andrias davidianus* skin secretion

Yuqing Liu,[1,10] Yinghao Li,[2,5,10] Haitao Shang,[4,10] Wen Zhong,[6] Quan Wang,[7] Kibret Mequanint,[8,9] Chuhong Zhu,[2,3,*] Malcolm Xing,[1,11,*] and Hong Wei[4,*]

SUMMARY

The widespread use of biological tissue adhesives for tissue repair is limited by their weak adhesion in a wet environment. Herein, we report the wet adhesion mechanism of a dry granular natural bioadhesive from *Andrias davidianus* skin secretion (ADS). Once contacting water, ADS granules self-assemble to form a hydrophobic hydrogel strongly bonding to wet substrates in seconds. ADS showed higher shear adhesion than current commercial tissue adhesives and an impressive 72-h underwater adhesion strength of ~47kPa on porcine skin tissue. The assembled hydrogel in water maintained a dissipation energy of ~8 kJ/m^3, comparable to the work density of muscle, exhibiting its robustness. Unlike catechol adhesion mechanism, ADS wet adhesion mechanism is attributed to water absorption by granules, and the unique equilibrium of protein hydrophobicity, hydrogen bonding, and ionic complexation. The *in vivo* adhesion study demonstrated its excellent wet adhesion and hemostasis performance in a rat hepatic and cardiac hemorrhage model.

INTRODUCTION

Adhesives for biological tissues have great perspectives in tissue repair and suture-free wound closure. Current tissue adhesives are generally comprised of synthetic polymers or natural macromolecules. Synthetic adhesives mainly include cyanoacrylates (Trott, 1997), polyethylene glycol (Elefteriades, 2009), and polyurethane (Su et al., 2019), which showed good adhesion but may present some drawbacks, such as cytotoxicity, slow biodegration, and inflammations{Trott (1997) #6}{Trott (1997) #6}. Nature-derived adhesives are mainly protein-based materials, such as fibrin (Spotnitz, 2010), gelatin, and elastin (Annabi et al., 2017; Guo et al., 2021; Liu et al., 2016; Wang et al., 2021), or polysaccharides (Sani et al., 2019), including alginate, chitosan, and hyaluronic acid (Li et al., 2017; Puertas-Bartolomé et al., 2019), which are generally biocompatible and biodegradable. The general adhesion mechanisms of tissue adhesives include intermolecular covalent bonding and intermolecular non-covalent bonding including hydrogen bonding, electrostatic interaction and hydrophobic intreaction, mechanical interlocking, and chain entanglement (Li et al., 2017; Mahdavi et al., 2008; Mehdizadeh and Yang, 2013; Steck et al., 2020). However, high adhesion capacity on wet tissue surface or in wet biological environment is still a huge challenge. To achieve high adhesion performance on wet biological substrates (Bouten et al., 2014; Feiner et al., 2016; Mehdizadeh and Yang, 2013; Sharma et al., 2013), the boundary water layer of body fluids or blood on the tissue surface, which hinders formation of strong adhesion, have to be displaced by bioadhesives. Several wet adhesion mechanisms and strategies were explored to remove surface water and improve interfical interactions to improve adhesion capacity in wet environment have been explored(Cui and Liu, 2021), including mussels-inspired adhesives through strong catechol bonding (Gao et al., 2020; Hofman et al., 2018; Lee et al., 2007a; Tiu et al., 2020; Zhang et al., 2020), dry double-sided hydrogel tape to absorb surface water (Yuk et al., 2019), entangled hydrophobic fluid gel to repel surface water and build covalent bonding (Liu et al., 2022b), underwater polyelectrolyte coacervate (Cui et al., 2019; Zhao et al., 2016), octopi/geckos biomimetic architecture physical adhesive repelling water through surface microchannels (Baik et al., 2017; Chen et al., 2020b; Lee et al., 2007b), instant tough bioadhesive(Chen et al., 2020a; Yang et al., 2018), multiple layer origami bioadhesive patch repelling fluid (Wu et al., 2021), hydrogel-mesh composite building covalent bonding on tissue surface (Gao et al., 2021), tough nucleobase-tackified adhesive (Liu et al., 2019a, 2019b), self-hydrophobization hydrogel with increased hydrophobic interaction to repel water

[1]Department of Mechanical Engineering, University of Manitoba, Winnipeg, MB R3T 2N2, Canada

[2]Department of Anatomy, Key Lab for Biomechanics and Tissue Engineering of Chongqing, Army Medical University (Third Military Medical University), Chongqing, 400038, China

[3]State Key Laboratory of Trauma, Burn and Combined Injury, Key Lab for Biomechanics and Tissue Engineering of Chongqing, Army Medical University (Third Military Medical University), Chongqing 400038, China

[4]Institute of Precision Medicine, The First Affiliated Hospital, Sun Yat-sen University, Guangzhou, Guangdong, 510080, China

[5]Chongqing Institute of Zhong Zhi Yi Gu, Shapingba District, Chongqing 400030, China

[6]Department of Biosystems Engineering, University of Manitoba, Winnipeg, MB R3T 2N2, Canada

[7]Department of Civil Engineering, Shantou University, Shantou 515063, China

[8]Department of Chemical and Biochemical Engineering, University of Western Ontario, London, ON N6A 5B9, Canada

[9]School of Biomedical Engineering, University of Western Ontario, London, ON N6A 5B9, Canada

[10]These authors contributed equally

[11]Lead contact

*Correspondence: zhuch99@tmmu.edu.cn (C.Z.), malcolm.xing@umanitoba.ca (M.X.), weihong63@mail.sysu.edu.cn (H.W.)

https://doi.org/10.1016/j.isci.2022.105106

(Han et al., 2020), and nanoparticles acting as connectors between polymer chains to achieve rapid adhesion (Rose et al., 2014). Notwithstanding the progress made to date, the challenges, including low instant adhesion, long curing time, complex procedure, poor water resistance, and biocompatibility, are still difficult to overcome simultaneously. Furthermore, adhesives of polyelectrolyte/thermoresponsive coacervates and physical adhesives with biomimetic architectures still lack strong adhesion and may need organic solvents(Dompé et al., 2019; Lee et al., 2007b; Liu et al., 2019a; Zhao et al., 2016). The instant adhesion of catechol-based or covalent bonding adhesives is not enough, and a longer reaction time is needed (Cui et al., 2019; Gao et al., 2021). Moreover, the adhesion performance of lots of wet adhesives may drop significantly over time in a wet environment because of inadequate water resistance (Cui et al., 2019; Han et al., 2020; Mao et al., 2020; Yuk et al., 2019). Therefore, those challenges still obstruct the clinic transition of bioadhesives, although existing wet adhesives showed various application prospects.

Although the excellent wet adhesion performance observed in mussels and sandcastle worms inspired the development of biomimetic underwater adhesives, there are still several natural materials hidden in the secrets of nature that are yet to be explored (Lee et al., 2007a). Here, we focus on *Andrias davidianus*, or "Chinese giant salamander," which is known as the "living fossil". *Andrias davidianus* belongs to the Cryptobranchidae family dating back to 350 million years ago and is the current largest aquatic amphibian (Gao and Shubin, 2003; He et al., 2018; Hou et al., 2004; Murphy et al., 2000). Its skin secretions contain abundant bioactive compounds showed antibacterial behavior (Guo et al., 2012; Wang et al., 2011), wound healing activities (Xi et al., 2012), prohealing properties (Dang et al., 2022), high hemostasis performance (Zhang et al., 2022), and was used as wound dressing materials (Liu et al., 2022a). Apparently, like sandcastle worms building underwater "concretes" through particle aggregation (Zhao et al., 2016), dry ADS particulates instantly glue together to form a hydrophobic water-insoluble hydrogel strongly bonding to wet substrates when contacting water (Mao et al., 2020), showing impressive underwater contact adhesion behavior. Although the utility of ADS as a tissue adhesive is recently described (Deng et al., 2019; Zhang et al., 2022), the mechanism of adhesion remains unexplored. Herein, we report that the mechanism of ADS underwater adhesion differs from sandcastle worms because limited hydration and self-assembly of the dry granular natural hydrogel are driven by a unique combination of hydrophobic aggregation, hydrogen bonding, and ionic interactions are the main causes for strong and instant adhesions. The self-assembled hydrogel from hydrated granulates is self-standing with good mechanical performance, and could be applied without additional patches/support. Interestingly, the dry ADS granular adhesive exhibited excellent *in vitro* and *in vivo* hemostasis activity, exhibiting its functional prospect in clinical applications as wet bioadhesives.

RESULTS

Underwater contact adhesion behavior of instantly self-assembled granular ADS hydrogels

As shown in Figures 1A and 1B, the *Andrias davidianus* skin produces emulsion-like secretions under stimuli. By lyophilization and subsequent grinding, the white mucus was gradually turned to dry ADS granules (the size is around 3–200μm, as shown in Figure S1), which exhibits outstanding underwater contact adhesion. When the non-sticky dry ADS powder contacted with water, it was hydrated and assembled into granular hydrogel instantly. Time-lapse microscopy showed ADS particles absorbed water to form a granular gel, and further self-assembled together into bulky gel rapidly (Figure S2 and Video S1). The SEM images of ADS hydrogel showed that ADS granular gel integrated to form a porous hydrogel morphology (Figure 1C). It was observed that the bulk ADS hydrogel was formed from the assembly of ADS granular hydrogel, which no longer kept the morphology of individual grains. Figure 1D showed that when the dry ADS powder was hydrated in water, it quickly assembled into a sticky hydrogel within ~20s, which could hold a pendant of 50 g, exhibiting a strong underwater instant adhesion performance (Figure S3 and Video S2). The instant underwater adhesion of ADS granular hydrogel is much higher than that from underwater coacervation of polyelectrolytes containing catechol groups in a short period of less than 1 min, and without the need for organic solvent in the process (Zhao et al., 2016). The size of the hydrogel did not change in water, suggesting the assembled ADS hydrogel controlled its swelling, which can avoid weakened mechanical performance and also enhance water-tolerant adhesion (Figures S4–S6). The assembled granular hydrogel fastened with two cotton threads can even hold a weight of 50 g underwater for 7 days without failure (Figures 1E and S7), showing its surprising underwater adhesion performance and good water resistance. The granular hydrogel has intrinsic self-adhesion by bridging head-to-head gel pieces within, and the jointed interface (1 × 15mm) sustained a weight of 20g normal adhesion stress without failure (Figures 1F, S8 and Video S3). The self-adhesion behavior of ADS granular adhesive increased the adhesion robustness, which was not reported for coacervation-based adhesives, as their macromolecular chain

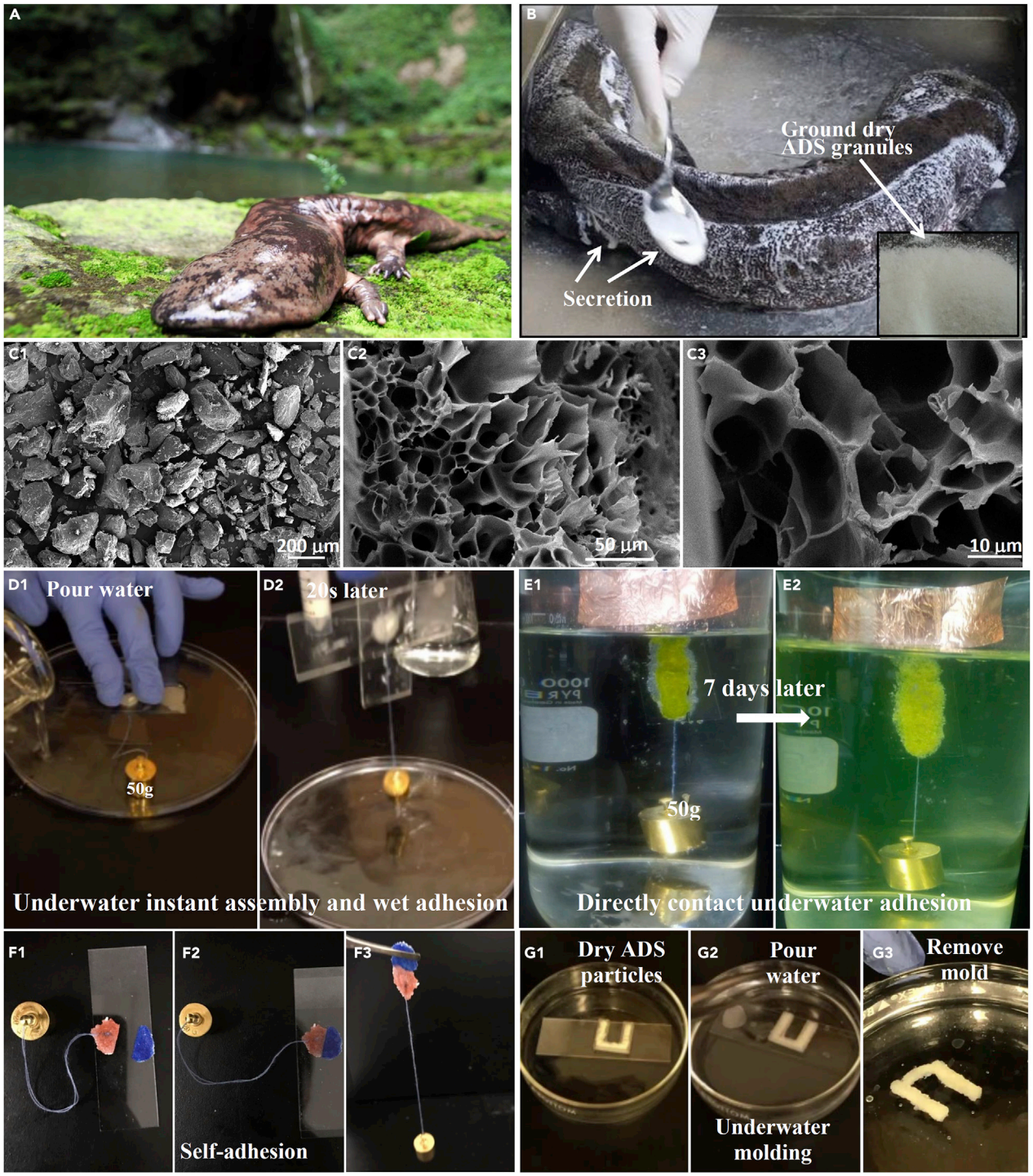

Figure 1. Underwater contact adhesion behavior of instantly self-assembled granular hydrogels from dry ADS particulates

(A) Digital photograph of an adult Andrias Davidianus.

(B) Digital photograph of the skin secretion collection (the inset shows ADS powders).

(C) SEM images of dry ADS granules (c1, scale bar: 200 μm) and self-assembled ADS granular hydrogel internal cross-section at different magnifications (c2 and c3, scale bar: 50 μm and 10 μm respectively).

(D) Instant self-assembly of ADS particulates to form an adhesive patch in water (E) 50 g weight handing from the hydrogel was soaked in water for up to 7 days (the color was from the fluorescein dye).

(F) Self-adhesion behavior of ADS hydrogel and the repaired patch could afford a weight of 20 g.

(G) Molding ADS into a U-shape hydrogel via self-assembly and self-adhesion.

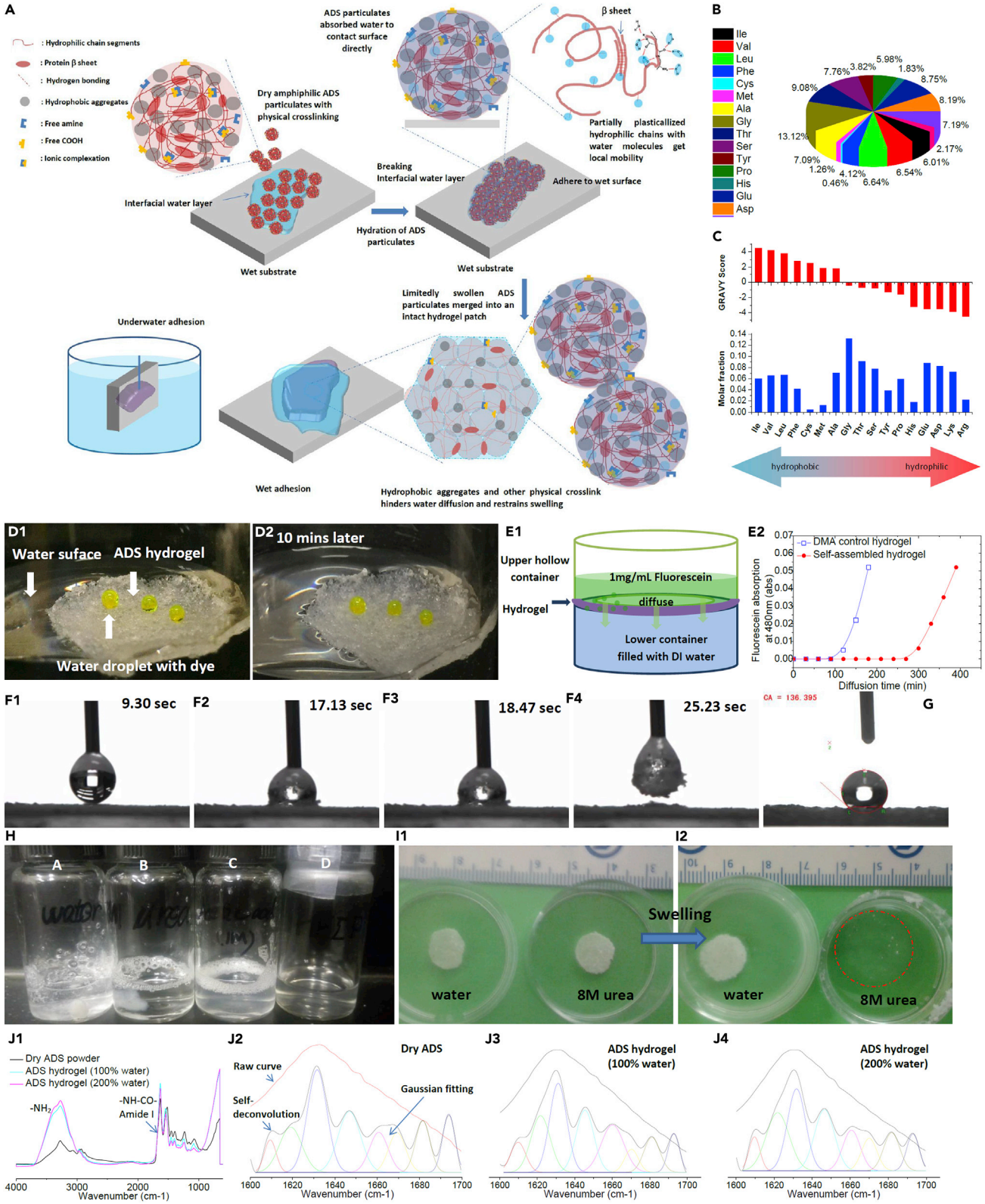

Figure 2. Wet adhesion mechanism of ADS

(A) Schematic illustration of dry ADS particulates' self-assembly and adhesion mechanism in water.

(B) The amino acid composition analysis of ADS proteins.

Figure 2. *Continued*
(C) The GRAVY score evaluation of ADS proteins.
(D) The hydrophobic behavior of self-assembled hydrogels floated on water.
(E) The diffusion behavior of fluorescein dye a.q. solution (1 mg/mL) passing through an ADS hydrogel patch or a control hydrogel (dimethylacrylamide, DMA) (thickness= 1mm).
(F) Hydration and hydrophobic self-assembly of ADS particles on the air-water interface of a water droplet.
(G) The water contact angle of a water droplet on ADS hydrogel surface.
(H) The solubility of ADS hydrogel (100% water-swollen, 20mg) in different solvents (1 mL). (A) water, (B) 8M urea a.q. solution, (C) 1M acetic acid solution, and (D) HFIP.
(I) The swelling behaviors of the ADS hydrogel (100% original swollen ratio) in water or 8M urea a.q. solution respectively.
(J1) The FTIR-ATR spectra of dry ADS powder and ADS hydrogel with different hydration levels (100% or 200%). The FTIR-ATR raw curves, self-deconvoluted curves, and corresponding Gaussian fittings in the amide I region of dry ADS powder (J2), 100% swollen ADS hydrogel (J3), or 200% swollen ADS hydrogel (J4).

mobility was lost after coacervation and solidification (Cui et al., 2019; Zhao et al., 2016). Thisself-assembly behavior of granular hydrogel in water can also assure preparing it underwater rapidly without heat or high pressure. As shown in Figure 1G, the ADS powder was filled into a U-shape mold, and the bulk hydrogel formed in less than 1 min by soaking with water (Figure S9 and Video S4). This self-assembly molding of granular hydrogel could offer a facile way to fabricate complex shapes.

Wet adhesion of ADS hydrogels

The ADS's composition was studied first at the molecular level. The major components found in ADS were proteins (accounting for ~90 wt %), polysaccharides (~6 wt %)and fatty acids (~4 wt %). There are ~150 proteins and 17 amino acids found in the secretion according to the proteomic analysis results (Data S1) (Geng et al., 2015). Because of the limited amount of catechol or other reactive groups such as thiols found in ADS and the total dissolution of ADS hydrogel in hexafluoroisopropanol (HFIP), the catechol chemistry or covalent bonding (disulfide) mechanism could be excluded. Instead, we hypothesized that the instant wet adhesion is of physical interactions attributed to the exquisite mixing of hydrophobicity, hydrophilicity, hydrogen bonding, and ionic complexation of ADS proteins (Figure 2A). Hydrophobic aggregation drives the self-assembly of ADS particles in water (Oliveira et al., 2016), whereas hydrophilic components are hydrated and plasticized instantly assemble the granular hydrogels and glue the substrate in position (Mao et al., 2020; Yuk et al., 2019). On a wet surface, an aqueous hydration layer obstructs direct contact between adhesives and substrate (Israelachvili and Wennerström, 1996), which will be absorbed by ADS hydration to achieve direct touch for strong wet adhesion (Yuk et al., 2019). Because of hydration, the hydrated hydrophilic chains become flexible and interpenetrated between adjacent granules and therefore "fused" them into an intact bulk. The SEM images (Figure 1C) of self-assembled ADS hydrogel showed typical porous structure without morphology of any individual ADS dry particles, suggesting the complete integration of ADS granular gels. The physical crosslink further restrains ADS hydrogel from swelling caused disassembly and thus to achieve strong underwater cohesion.

The amino acid analysis (Figures 2B and 2C) confirms the amphiphilic compositions of ADS proteins, which were evaluated as ~-0.2 through grand average of hydropathicity (GRAVY) estimation (Tables S1 and S2) (Kyte and Doolittle, 1982). Figure 2D presents the high hydrophobicity of assembled ADS hydrogel. The dye-colored water droplets spherically stood on ADS hydrogel which was freely floating on the water surface. The water droplets retained their shape with high water contact angle over for 10 min without wetting ADS hydrogel surface. Figure 2E shows that the sodium fluorescein dye solution diffused much slower through ADS hydrogel than poly(dimethylacrylamide) hydrogel (PDMA, crosslinked by N,N'-methylenebisacrylamide at the same thickness and concentration). Compared with the non-ionic hydrophilic PDMA gel, the self-assembled ADS granular hydrogel significantly retarded the diffusion of the sodium fluorescein salt solution because of its hydrophobicity and abundant intermolecular ionic interactions.

Figure 2F (Video S5) exhibits the ADS particulates dynamically adsorbed onto the water droplet surface, then quickly self-assembled to form an ultra-thin gel layer, because the gel hydrophobicity kept granules from further diffusion inward. The ADS hydrogel of 100wt % swelling ratio had a water contact angle of $132.1 \pm 3.0^{\circ}$, showing its high hydrophobicity (Figures 2G and S10). Under a real-time optical microscope, dry amphiphilic ADS granules were observed instantly hydrated to form an insoluble hydrogel.

To understand the influence of ADS particles' size, ADS particles were prescreened to two groups through the mesh of ~250 μm, ADS-large and ADS-small groups. The size distributions of ADS-small and ADS-large

are 3–160 μm and 50–550 μm respectively. For the ADS-large group, small size particles (diameter <50 μm) were ignored as their volume percentage in the ADS-large group is low, as shown in Figures S11A–S11E. It was found that the overall water swelling ratio of two groups kept similar, suggesting similar hydrophobicity and hydrophilicity, as ADS-large and ADS-small have same chemical compositions (Figure S11F). Although the water-absorption rate of ADS-small is obviously higher than that of ADS-large particles in first 5 min of soaking, which should be because of the surface area of small size particles are typically higher than that of large particles, leading to higher absorption rate at early stage. The water contact angle of ADS hydrogel patches from ADS-large are 137.4 ± 1.8°, which is significantly higher than that of ADS-small hydrogel patches, 127.1 ± 1.8° (Figures S11G–S11I). This should be attributed to the higher surface roughness of the hydrogel patch from assembly of large particles. The pore sizes of ADS hydrogels from ADS-large or ADS-small are similar, as shown in Figure S12. The hydrogel patches comprised of ADS-large particles or ADS-small particles have similar pore size distribution of 1–160 μm, which is reasonable as ADS-small and ADS-large hydrogel patches have similar water swelling ratio when balanced.

As a comparison, the behaviors of water-insoluble polymer (chitosan powder; > 400mPas) and water-soluble polymer (sodium alginate) were also studied (Figure S13). Chitosan has a similar structure to polysaccharides with abundant amine groups, which could be dissolved in acidic solution but not in neutral pH (Lee et al., 2013). Water soluble sodium alginate powder was selected as water soluble particulate model, which has a polysaccharide structure with carboxylate groups and therefore good solubility in water. As shown in Figures S13A and S13B, water-insoluble chitosan particulates floated and self-assembled on the waterfront but never adhered together because the rigid biomacromolecular chains were not hydrated and plasticised with water to obtain high chain mobility, whereas the hydrophilic sodium alginate particulates were hydrated first but soon completely dissolved (Figure S13C). The proper amphiphilicity is critical to balance the interface adhesion and underwater cohesion. Because the main composition of ADS is amphiphilic proteins, containing abundant hydrogen bonding and ionic charges, multiple non-covalent interactions were taken into consideration, including hydrophobic interaction, hydrogen bonding and ionic complexation. To further confirm the type of interactions in ADS hydrogel, four types of solutions, water, urea a.q. solution (8M), acetic acid a.q. solution (1M), and HFIP, were tested to swell or dissolve ADS hydrogels. ADS gel (∼20 mg, weight ratio of ADS and water = 1:1) was placed in a glass vial, and 1mL of selected solvent was added. The glass vial was vortexed for a few minutes and placed at ambient temperature for 1 h. The ADS hydrogel maintained its shape and was insoluble in water. In urea solution, the gel was insoluble but swollen, because the urea molecules were favorably competitive over hydrogen bonding of ADS to form the intermolecular H-bond with ADS through introduced carbonyl diamide functional groups, and the swelling ratio of the hydrogel in urea solution was over 2-folds of that in water (Figure 2I). The ADS hydrogel was completely disassembled in 1M acetic acid a.q. solution, appeared cloudy, suggesting the existence of insoluble microparticles or micelles from the hydrophobic aggregates of ADS. The acetic acid molecules could break both ionic and hydrogen bonding interactions in ADS, but not hydrophobic aggregations. ADS hydrogel was completely dissolved in HFIP, because HFIP contains both hydrophilic groups of hydroxyls and hydrophobic fluorocarbons, and therefore can dissolve the both hydrophilic and hydrophobic components of ADS completely. The dissolution and disassembly behavior of ADS hydrogel suggests that its self-assembly and wet adhesion mechanism should be attributed to non-covalent interactions of hydrogen bonding, ionic complexation and hydrophobic interaction.

For underwater cohesion, a high mixing free energy of ADS with water ($\Delta G > 0$) and a high enthalpy (Equations 1 and 2) are required. Hansen solubility parameter of ADS proteins were calculated to estimate the cohesive energy contributions of atomic dispersion force (δ_d), dipole-dipole interaction force (δ_p), and hydrogen bonding interaction (δ_h) (Equation 3)(Hansen, 2007). The calculated δ_d;$\delta_p\delta_h$ values of ADS proteins are 17.78; 11.14; 11.54 $MPa^{1/2}$ (Tables S3, S4 and Data S2), suggesting the important contribution of protein nonpolar interactions to its cohesive energy and high mixing enthalpy because of huge dissimilarity with water(δ_t:47.9, δ_d : 12.9) (Barton, 2017).

$$\Delta G_{mix} = \Delta H_{mix} - T\Delta S \quad \text{(Equation 1)}$$

$$\Delta H_{mix} = V\varnothing_1\varnothing_2\left[(\omega 1 - \omega 2)^2 + (\Omega 1 - \Omega 2)^2\right] \quad \text{(Equation 2)}$$

$$\text{Total solubility parameter: } \delta_t = \left(\delta_d^2 + \delta_p^2 + \delta_h^2\right)^{1/2} \quad \text{(Equation 3)}$$

The intermolecular hydrogen bonding and ADS proteins secondary structures were analyzed in the amide band I region of FTIR-ATR spectra (Figure 2J) (Jackson and Mantsch, 1995). In a dry state, the fraction of β and antiparallel β sheet accounted for 53.34% of total secondary structures, showing strong intermolecular hydrogen bonding interactions. After the formation of the hydrogel, the value was 53.29% for 100% hydration (water swelling), or 54.51% for 200% hydration, suggesting that water neither disassembled the β sheet aggregates nor broke the intermolecular hydrogen bonding network (Xu et al., 2017), but could be broken by urea molecules as discussed above (Tables S5–S7).

Figure 3A shows the schematic illustration to interpret the ionic complexation interactions in ADS hydrogel. In 1 M acetic acid solution, a 5wt% of ADS (disassembled to form a cloudy emulsion, as excessive acetic acid molecules broke protein inter/intrachain ionic complexation and hydrogen bonding. Mixed with 1wt % sodium alginate solution, the crosslinked network of ionic complexation and new hydrogel re-formed, with increased storage modulus (G′), loss modulus (G″), and viscosity, demonstrating the contribution of ionic complexation to ADS underwater cohesion, as shown in Figures 3B–3D. In the frequency sweep profiles of ADS hydrogel, both G′ and G″ dropped significantly with an increase of water swelling ratio because of a decrease in physical crosslink density, as shown in Figure 3E. The self-adhesion behavior of ADS granular hydrogel was also characterized as shown by the oscillation frequency sweeping results of the ADS granular hydrogel before cutting and after recovery (Figure 3F). The self-adhered hydrogel exhibited similar dynamic behavior with 20–30% loss in both G′ and G′′. The alternate strain cycling test (0.1% or 100%) was conducted for ADS hydrogels, as shown in Figure 3G. During the whole period, G′ was always higher than G″, without any sign of solid-liquid transition under high strain shearing condition, as typical self-healable materials. So the recovery of the cut patches was considered as self-adhesion at the macroscopic level. It also suggests that granular assembled ADS hydrogel kept good stability without physical-network disassembly or reconstruction under a highly dynamic environment, which is necessary for soft tissue adhesives applied to biological tissues where dynamic movements happen.

To evaluate the underwater cohesion of ADS bulk hydrogel, the dissipated cohesion energy of hydrogels with different swelling ratios was measured according to Equation 4 (Figures 3H and 3I).

$$\Delta U = \int_1^{\lambda_c} \sigma_{loading} d\varepsilon - \int_1^{\lambda_c} \sigma_{unloading} d\varepsilon \qquad \text{(Equation 4)}$$

There is good linearity between dissipated energy and the solid content in ADS hydrogels (Figure 3J), suggesting the underwater cohesion is proportional to hydrogel solid content (inversely proportional to swelling ratio). Thus, the higher the swelling ratio of the assembled ADS hydrogel the weaker its underwater cohesion, and the hydrophobicity could prevent ADS hydrogel from dissembling in water. Based on the linear fitting and the swelling behavior, the minimum dissipated energy of fully swollen ADS hydrogel in water is calculated as ~8 kJ/m^3, which is comparable to the work density of muscle tissue (Ma et al., 2020; Mirfakhrai et al., 2007), suggesting its robustness for tissue adhesion applications in wet environment. With the same swelling ratio, the ADS hydrogel in 8M urea showed much less cohesion energy because of the weakened intermolecular hydrogen bonding network by urea molecules (Figure 3K). Therefore, it could be concluded that the exquisite hydrophobicity/hydrophilicity, hydrogen bonding, and ionic complexation of ADS proteins contribute to the self-assembly and adhesion performance of ADS granular gels, and the dry ADS powder could remove the surface water barrier to contact substrate closely and build strong adhesion by water absorption.

Instantly assembled ADS granular hydrogel on porcine skin tissue could afford dynamic stretching and twisting and a normal force of 500 g without any failure in the perpendicular direction of the substrate (Figures 4A, 4B and Video S6). ADS particulates self-assembled to form a hydrogel patch that tightly adhered to liver tissue in the presence of blood (Figure 4C and Video S7). To evaluate the adhesion capacity of ADS hydrogel, its lap shear adhesion on two flexible substrates, porcine skin tissues and PDMS, was measured (Figure S14). ADS hydrogel showed the highest lap shear adhesion of 80.8kPa ±8.8 kPa on porcine skin surface, compared with two commercial tissue adhesives, cyanoacrylate and fibrin glue (Figures 4D–4G). Although the adhesion was much less on the hydrophobic PDMS surface because of little ionic complexation and hydrogen bonding, ADS hydrogel still showed the best performance among all tested groups. The ADS hydrogel also showed the highest normal adhesion performed on stainless steel plates compared to fibrin and cyanoacrylate glues (Figure S15). Considering the ionic interaction from the negative charges of tissue surfaces is a factor in ADS adhesion, a carboxylic acid decorated PDMS surface (PDMS-COOH) was prepared for validation (Scheme S1). ADS adhesion was significantly enhanced on

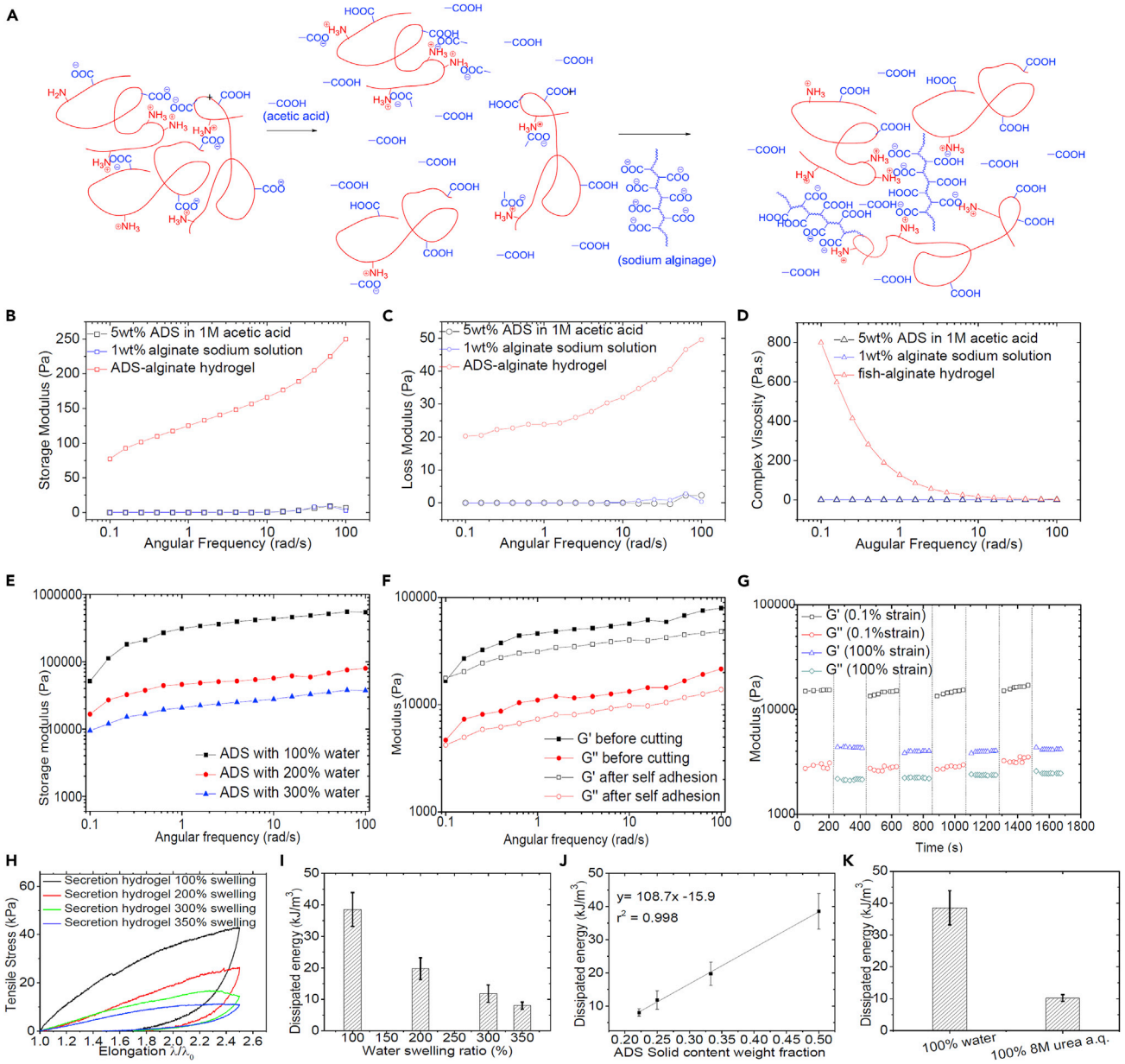

Figure 3. Physical crosslinking in ADS hydrogel

(A) Schematic illustration of ionic complexation contribution in ADS hydrogel.

(B–D) The rehological profiles of 5wt% ADS in 1M acetic acid solution, 1wt% alginate aqueous solution, and the mixture of ADS-acetic acid/alginate solution in oscillation frequency sweeping test, including storage modulus vs. angular frequency (B), loss modulus vs. angular frequency (C) and complex viscosity vs. angular frequency (D).

(E) Frequency sweep rheological profiles of ADS hydrogel with different swelling ratios (100, 200, and 300%).

(F) Frequency sweep test of ADS hydrogel before cutting and after self-adhesion.

(G) The dynamic strain amplitude alternating cyclic test of ADS hydrogel at the shearing rate of 1 rad/s, the strains were shifted between 0.1% or 100% for 8 steps (4 cycles), and the period per step was 200 s.

(H)The tensile stress-strain cycle curves of ADS hydrogels with different swelling ratios.

(I) The dissipated energy of ADS hydrogels with different swelling ratios (n = 3).

(J) The linearity of dissipated energy vs. ADS solid content (n = 3).

(K) Comparison of dissipated energy between ADS hydrogels swollen with 100% water or 8M urea a.q. solution (n = 3).

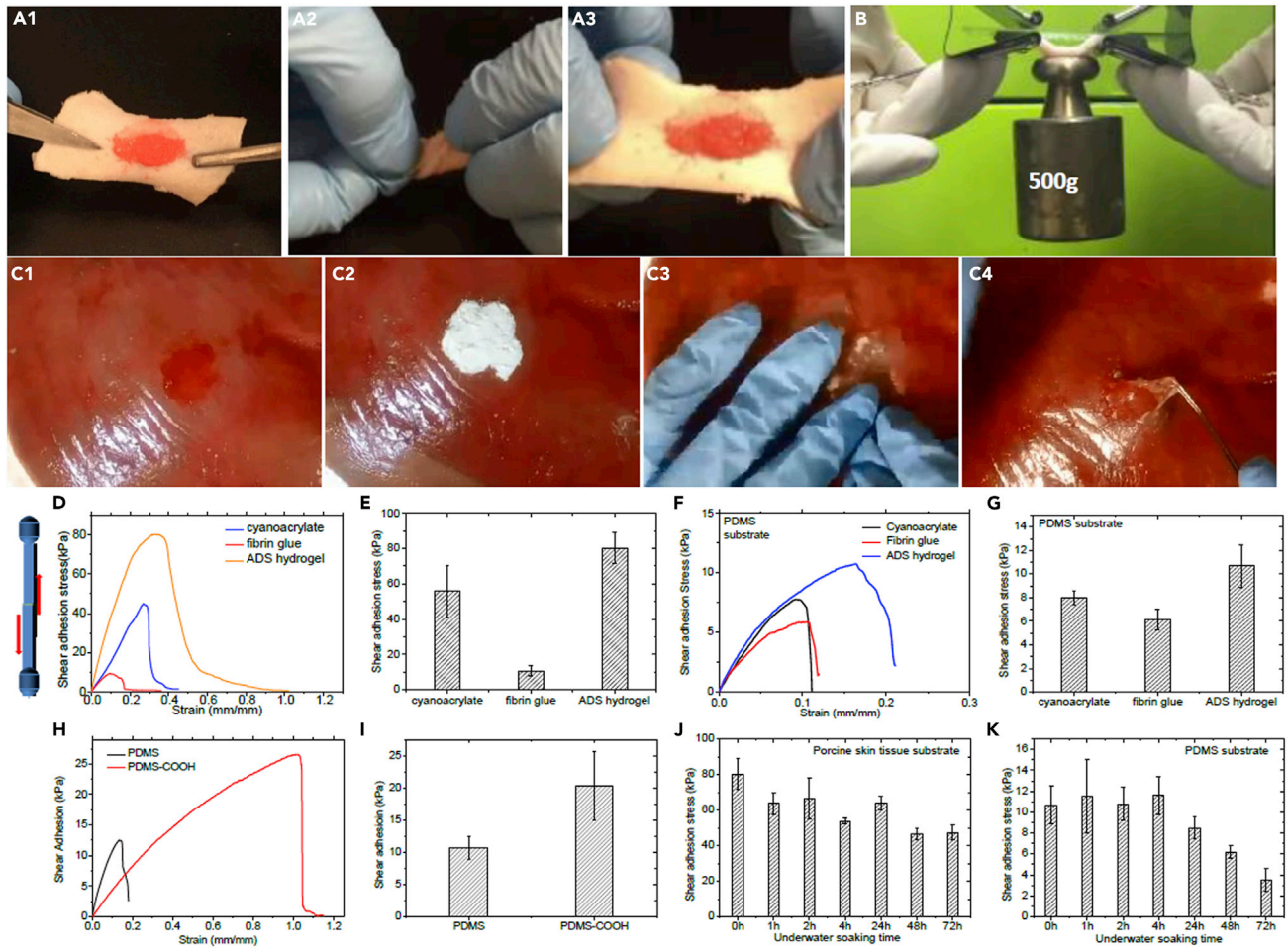

Figure 4. The adhesion performance of ADS hydrogel

(A) ADS hydrogel adhered to porcine skin tissue twisted and restored.

(B) ADS hydrogel formed on porcine skin tissue surface bearing a weight of 500 g.

(C) ADS hydrogel *in-situ* formed and adhered to the porcine liver surface via self-assembly.

(D and E) Lap shear adhesion stress of ADS hydrogel, cyanoacrylate, and fibrin glue on porcine skin tissue substrate (n = 3).

(F and G) Lap shear adhesion stress of ADS hydrogel, cyanoacrylate adhesive, and fibrin glue on PDMS substrate (n = 3).

(H and I) Lap shear adhesion of ADS hydrogel on regular PDMS or carboxylic acids decorated PDMS (PDMS-COOH) surface (n = 3).

(J and K) Underwater contact adhesion of ADS assembled hydrogel on porcine skin tissue and PDMS substrate surface (n = 3).

PDMS-COOH surface, further confirming the contribution of ionic complexation (Figures 4H, 4I, S16 and S17). The underwater contact adhesion performance of ADS hydrogel was examined by underwater soaking up to 72 h. The ADS hydrogel soaked in water maintained ~80% adhesion capacity on porcine skin tissue after 24 h, and ~65% of its initial performance after 72h (~47kPa), exhibiting an outstanding underwater contact adhesion capacity. On a PDMS surface, the adhesion in water dropped considerably, but still had 35% residual capacity after 72h (Figures 4J and 4K).

To further confirm the adhesion mechanism of ADS granular hydrogel, an amphiphilic model biomacromolecule containing both free amine groups and carboxylic acid groups, O-carboxymethyl chitosan (CM-chitosan), was synthesized. In doing so, its hydrophobicity was further enhanced by the introduction of methacrylate groups on CM-Chitosan (CM-Chitosan-MA), as shown in Figures 5A (Figures S18 and S19). The lyophilized CM-chitosan-MA solid was ground to a fine powder under liquid nitrogen, which showed an interesting self-assembly behavior in water similar to ADS granules. Mixed with equal amount of water, CM-chitosan-MA particulates assembled in less than 1 min and afforded a weight of 500 g successfully on a glass substrate, exhibiting significantly improved adhesion capacity (Figure 5B). By introducing the extra

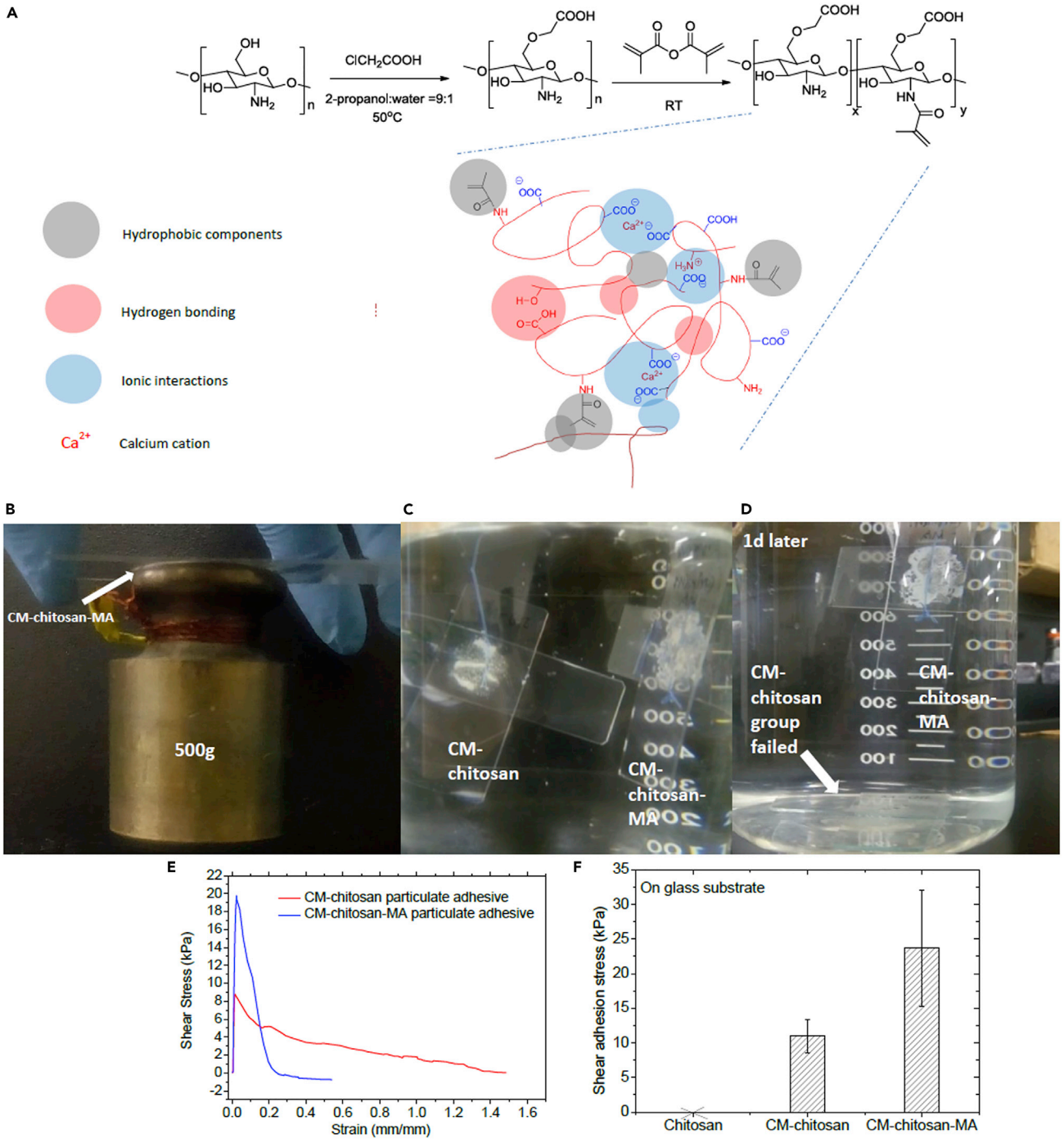

Figure 5. Synthetic model polymer methacrylated carboxymethyl chitosan (CM-chitosan-MA) granular adhesive to mimic the wet adhesion behavior of ADS hydrogel

(A) The designed model polymer, CM-chitosan-MA, based granular hydrogel adhesive.

(B) CM-chitosan-MA particulates with 100% water self-assembled to a hydrogel patch to hold a weight of 500 g on a glass substrate.

(C and D) Underwater adhesion performance of CM-chitosan-MA particulates and CM-chitosan particulates (control group).

(E and F) Lap shear adhesion of CM-chitosan-MA and CM-chitosan hydrogels on glass substrates. Note: with water, chitosan particles could not assemble and could not adhere to substrates (n = 3).

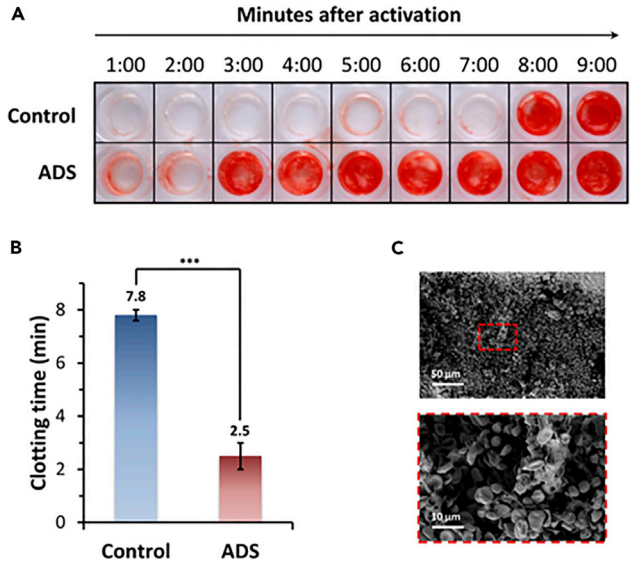

Figure 6. Characterization of the procoagulant effect of ADS on the whole blood

(A) Qualitative analysis of blood clotting with or without ADS powder treatment in 96-well plates.

(B) Quantification of clotting time of whole blood in contact with ADS powder compared to control group. Data are means ± SD (n = 3). p value determined by Student's *t*test (***p < 0.001).

(C) SEM analysis of the interaction of ADS with red blood cells (RBCs, scale bar: 50 μm and 10 μm respectively).

ionic complexation of calcium ions, the gel showed strong underwater adhesion behavior as well. 50-mg CM-chitosan-MA particulates or CM-chitosan particulates (control group) were mixed with 50μL of 0.5M $CaCl_2$ solution (100% swelling) to form hydrogel patch and adhered to two glass slides, which were hanged and soaked in water, as presented in Figure 5C. After one day, the CM-chitosan-MA hydrogel patch still successfully held two glass slides through a cotton thread underwater, whereas the control group CM-chitosan without hydrophobic MA components failed soon, as shown in Figure 5D. The lap shear adhesion results in Figures 5E and 5F also showed the obvious improvement of adhesion performance of hydrophobically modified particulates, suggesting a feasible approach to improve adhesion capacity and wet adhesion performance.

Hemostatic properties of ADS hydrogels

To evaluate the hemostatic performance of ADS hydrogels, we first investigated the *in vitro* procoagulant effect of ADS on whole blood (Figure 6). As shown by plate assay (96-well), the clotting process of ADS-treated blood was accelerated remarkably in comparison with the control (Figure 6A). Quantitative analysis of blood clotting time showed that the mean coagulation time of the ADS group was 2.5 ± 0.5 min, which is much shorter than 7.8 ± 0.2 min for the control group (Figure 6B). Morphological analysis of the ADS-blood components complex by SEM (Figure 6C) confirmed that the red blood cells (RBCs) were rapidly aggregated to form a 3D network structure with ADS and transformed biconcave shapes into polyhedral shapes upon ADS interaction.

We further probe the *in vivo* hemostatic performance of ADS hydrogel on a liver hemorrhage model (Figures 7A, S20 and Video S8). A severe laceration on the lobe of rat liver was created with scalpel (Figures 7A1 and A2), and then dry ADS powder was applied to the lesion region immediately (Figure 7A3). With the hydration and instant self-assembly of ADS powder on the bleeding liver surface, a free standing hydrogel layer was formed to cover the wound site, which showed strong wet adhesion and cohesion and efficiently stopped the bleeding in 1 min without applying an extra patch (Figures 7A4 andA5) whereas in the untreated group, bleeding was nearly uncontrollable without treatment (Video S9). The hemostatic capacity of ADS hydrogel was further evalauated in heart hemorrhage model (Figures 7B and Video S10). As shown in Figures 7B1 and 7B2, the ventriculus sinister of the rat heart was punctured by a needle of 1 mm diameter, leading to bleeding, which was immediately treated with ADS powder (Figure 7B3). The puncture wound was sealed robustly following ADS hydration and assembly (Figures 7B4 and 7B5). The SEM images revealed that a sealing layer with 3D microporous network was formed at the interface between ADS powder and wound tissues (Figures 7C and 7D). A large number of

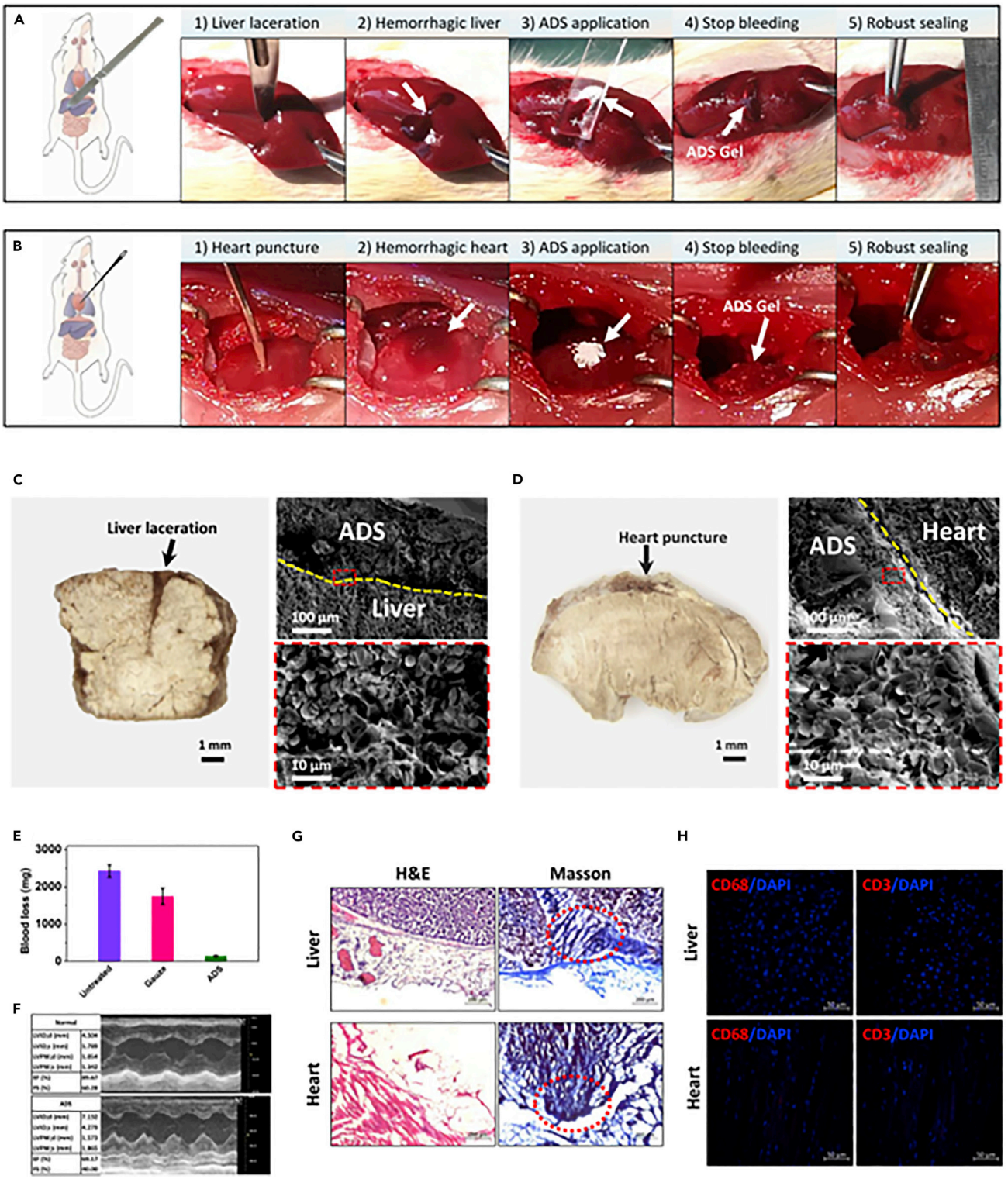

Figure 7. Hemostatic performance of ADS hydrogel in rat's hepatic and cardiac hemorrhage model

(A and B) The rapid hemostasis and sealing process of ADS hydrogel for rat liver laceration (A) and heart puncture (B); (C and D) Photographic (left) and SEM (right) images of freeze-fractured ADS-tissue interface for injured liver (C) and heart (D) tissues. The interfaces were marked with a dotted yellow line (scale bar: 1mm (left), 100 μm (right top), and 10 μm (right bottom) respectively).

(E) Quantification of blood loss for lacerated liver treated with ADS hydrogel, gauze and control (untreated) (n = 3).

Figure 7. *Continued*

(F) Echocardiography measurements of normal and ADS-treated groups after 4 weeks.

(G) Histology images of ADS hydrogel and the around injured tissue stained with H&E and Masson's trichrome after 4 weeks of treatment (scale bar: 200 μm).

(H) Immunostaining images (DAPI, CD3 and CD68 marker) of injured tissue treated with ADS hydrogel after 4 weeks (scale bar: 50 μm).

RBCs were activated, aggregated and encapsulated into the network, which demonstrated ADS as the effective physical barrier for hemostasis. During the treatment, the blood loss was also carefully collected with a filter paper to quantify the hemostatic efficiency of ADS hydrogel (Figure S18). In comparison with the untreated group, the blood loss was significantly reduced in the ADS-treated group, and the hemostatic efficacy of ADS reached ~94%, which is superior than the gauze-treated group which showed only ~28% hemostatic efficacy (Figure 7E). In addition to the timely hemostatic effect at an early stage, the repair capacity of the ADS hydrogel at late stage was also probed. After 4 weeks, all animals survived without secondary hemorrhage in rat hepatic and cardiac hemorrhage model. Evaluation of cardiac function by echocardiography measurements revealed that of ADS-treated group did not have a marked decrease in the ejection fraction (EF) and fractional shortening (FS) values, and maintained similar left ventricle (LV) geometry compared to the normal group (Figure 7F). Furthermore, the host immune response of ADS hydrogel in rat models of hepatic and cardiac hemorrhage was evaluated. Histological analysis and immunostaining for macrophages (CD68) and lymphocytes (CD3) showed that only slight lymphocytes ($CD3^+$) and macrophages ($CD68^+$) infiltration was observed after 4 weeks of ADS treatment, which indicates no apparent local host inflammatory response for this foreign secretion (Figures 7G and 7H). The *in vivo* biocompatibility, biodegradation and immunogenicity of the ADS were further evaluated by subcutaneous implantation in a rat model of dorsal subcutaneous implantation (Figures 8A and 8B). Histological assessment demonstrates that after 1 week of implantation, ADS hydrogel generates moderate inflammatory reaction with the degradation of matrix network (Figure 8C, top). The infiltrated inflammatory cells are dispersed in the network structure. At 2 weeks of implantation, ADS hydrogel degrades significantly with the resolution of inflammatory response (Figure 8C, middle). The inflammatory cells retreat to the interacted tissue interface. At 4 weeks of implantation, the inflammatory cells are nearly disappeared (Figure 8C, bottom). There was no fibrous capsule formation or tissue necrosis during the whole treatment stage. The immunogenicity of ADS was also demonstrated in the related publication (Deng et al., 2019). These results demonstrated that ADS was highly biocompatible for wound treatment.

DISCUSSION

This study reports a natural hydrogel bioadhesive, dry amphiphilic protein granules from *Andrias davidianus* skin secretions, which could instantly self-assemble to form integrated hydrophobic bulky hydrogel in wet environment with strong wet adhesion and good water resistance. The interesting self-assembly and wet adhesion behavior of the ADS dry granules were unlike that of current popular wet adhesion bioadhesives using catechol bonding or underwater polyelectrolyte coacervate, and therefore the mechanism of ADS adhesive were studied and discussed.

Understanding self-assembly and wet adhesion mechanism of ADS granular adhesive

To elaborate on the self-assembly and integrated adhesion mechanism, the compositions of ADS was first investigated, which contains ~90wt % proteins, ~6wt % polysaccharides and ~4wt % fatty acids. With proteomic analysis results (Data S1), the amount of catechol and thiol reactive groups in ADS is low, and ADS hydrogel could be completely dissolved in HFIP, suggesting there is not any covalent bonding crosslinking. Therefore, the interesting self-assembly and integrated adhesion should be attributed to physical interactions, which may include the hydrophobicity/hydrophilicity, hydrogen bonding, and ionic complexation.

The amino acid analysis and GRAVY evaluation (Figures 2B and 2C) exhibited amphiphilic performance of ADS proteins, which was further proven by water swelling and water contact angle test. Water swelling test showed the hydrophilicity of ADS, which could absorb up to ~375wt% of water; and water contact angle showed its hydrophobicity with the water contact angle of 132.1 $\pm$ 3.0°, suggesting its amphiphilicity. The amphiphilicity is critical for the self-assembly and adhesion of ADS. On a wet surface, an aqueous hydration layer obstructs direct contact between adhesives and substrate (Israelachvili and Wennerström, 1996), which will be absorbed by ADS hydration to achieve direct touch for strong wet adhesion (Yuk et al., 2019). Because of hydration, the hydrated hydrophilic chains become flexible and interpenetrated between adjacent granules and therefore "fused" them into an intact bulk. The SEM images (Figure 1C) of self-assembled ADS hydrogel showed typical porous structure without morphology of any individual ADS dry particles, suggesting the complete integration of ADS granular gels. Although the hydrophobic

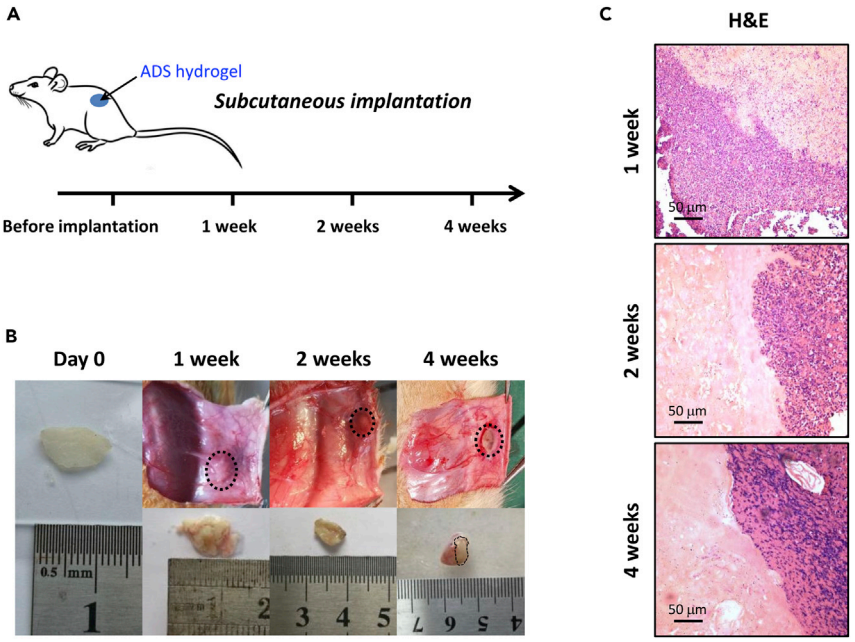

Figure 8. *In vivo* biocompatibility and biodegradability evaluation

(A) Schematic of ADS implantation in the rat dorsal subcutaneous pocket.

(B) Macroscopic appearance of ADS hydrogel pre-implantation and post-implantation excised at 1, 2 and 4 weeks.

(C) Histological images of ADS hydrogel implants and surrounding tissues after 1, 2 and 4 weeks after implantation (scale bar: 50 μm).

components could provide a physical crosslinking because of hydrophobic aggregations, which provided strong cohesion and good stability for the formed ADS hydrogel bulk in the wet environment.

The types of physical interactions were further discussed, which provided ADS hydrogels with good interfacial adhesion and underwater cohesion. As the main composition of ADS is amphiphilic proteins, containing abundant hydrogen bonding and ionic charges, multiple non-covalent interactions were taken into consideration, including hydrophobic interaction, hydrogen bonding and ionic complexation. Water, urea solution, acetic acid solution, and HFIP, were tested to swell or dissolve ADS hydrogels. Compared with water, the ADS gel in urea solution was further swollen but not dissolved. Urea molecules broke hydrogen bonding in ADS gels and leaded to further swelling (Figure 2I), but there are other interactions keeping the cohesion of ADS gels. The ADS hydrogel was completely disassembled in acetic acid solution, which broke both hydrogen bonding and ionic complexation of ADS. The solution appeared cloudy, suggesting existence of insoluble microparticles or micelles from the hydrophobic aggregates of ADS. ADS hydrogel was completely dissolved in HFIP, which can dissolve both hydrophilic and hydrophobic components of ADS completely. The analysis in the amide band I region of FTIR-ATR spectra (Figure 2J) suggested over 50% of total secondary structures in dry ADS and ADS gels are β sheet, showing strong hydrogen bonding in ADS gels. Figure 3A shows the schematic illustration to interpret the ionic complexation interactions in ADS hydrogel. The change of rheological profiles of ADS solution without or with acetic acids further confirmed the presence of strong ionic complexation in ADS (Figures 3B–3D).

Therefore, it could be concluded that the exquisite hydrophobicity/hydrophilicity, hydrogen bonding, and ionic complexation of ADS proteins contribute to the self-assembly and adhesion performance of ADS granular gels, and the dry ADS powder could remove the surface water barrier to contact substrate closely and build strong adhesion by water absorption.

Hemostatic mechanism of dry ADS granular adhesive

The hemostatic performance of ADS granules should be attributed to both its self-assembly driven by its amphiphilicity and the compositions of proteins. When ADS powder is applied to bleeding sites, the dry powder will absorb the fluid in the whole blood and self-assemble to form a layer of hydrophobic hydrogel patch within 20 s, which will adhere to the wound sites to block bleeding. On one hand, the dry ADS granules

absorbed blood, which removed blood and the surface liquid layer on the wound site to build strong bonding interactions and adhered to wound sites. On the other hand, the self-assembled bulky ADS hydrogel due to absorbing blood would block the wound site to stop bleeding and the hydrophobicity of ADS hydrogel further stopped the permeation of blood as a physical barrier. So, dry ADS powder could promote hemostasis through a physical approach. The absorption of the fluid components in the whole blood by ADS dry powder will also lead to aggregation of plasma proteins. From the view of chemical compositions, the major components in ADS are proteins, containing large amount of carboxylic acid groups and amine groups. Charge-based coagulation has also been applied to achieve rapid hemostasis (Avery et al., 2016; Gaharwar et al., 2014). The widespread charge on ADS protein can concentrate procoagulant factors around the adhesive hydrogel to realize coagulation and hemostasis. Moreover, ADS can also interact directly with cellular components in blood as the presence of cellular receptor proteins to promote hemostasis. The SEM images of the complex of ADS granules (Figure 6C) and blood suggested that the red blood cells (RBCs) were aggregated with ADS to form a 3D network structure and transformed the biconcave shape into the polyhedral shape upon ADS interaction. Thus, the unprecedented hemostatic ability of ADS is derived from the synergistic effect of its physical adhesion barrier and the procoagulant activity.

In conclusion, the interesting wet adhesion and water resistance of granular ADS adhesives are attributed to its unique amphiphilic protein composition, hydrogen bonding, and ionic complexation. The *in vivo* study demonstrated that dry ADS particulates could absorb water and self-assemble to form hydrogel sticking to wet tissues rapidly, which efficiently stopped blooding of punctured wound sites on livers and hearts without side effects. Because of the excellent adhesion capacity, rapid solidification via self-assembly, remarkable hemostasis performance and water-resistance, and good bio-compatibility and degradability, the ADS dry powder could be a promising surgical glue and hemostatic material for wound closure and tissue repair. It could be especially used for the emergent scenarios of severe bleeding and instant closure of wounds in wet conditions. Moreover, the granular particles can form any kind of shape via self-assembly and therefore could be used to handle wounds with irregular shapes in different positions.

Limitation of the study

In this study, the ADS granular adhesives are animal origin biomaterials from the skin secretions of adult *Andrias davidianus*. The cyctotoxicity, biocompatiability, and safety of these ADS granular adhesives should be investigated and evaluated more strictly for clinical trial and applications in the future, compared with plant origin biomaterials. Currently, the wet adhesion and hemostasis performance on biological tissue were assessed on rat hepatic and cardiac hemorrhage models only. The adhesion, hemostasis, and wound healing performance on other imporant tissues and organs, such as damaged lungs, arteries, and so on, are also challenges for the clinical applications of bioadhesives. Also, large animal models such as dogs and pigs should be employed for more detailed evaluation in the future.

STAR★METHODS

Detailed methods are provided in the online version of this paper and include the following:

- KEY RESOURCES TABLE
- RESOURCE AVAILABILITY
  - Lead contact
  - Materials availability
  - Data and code availability
- EXPERIMENTAL MODEL AND SUBJECT DETAILS
  - *In vivo* biocompatibility and biodegradability evaluation of ADS hydrogel
  - *In vivo* application of ADS hydrogel in a rat liver injury model
  - *In vivo* application of ADS hydrogel in a rat heart injury model
- METHOD DETAILS
  - *Andrias davidianus* secretion (ADS)
  - Lap shear adhesion test
  - Cohesive energy of ADS the granular hydrogel with different swelling ratios
  - SEM characterization
  - FTIR identification of ADS secondary structure fractions
  - Rheological characterization
  - Wet adhesion behavior of self-assembled ADS hydrogel

- Optical microscope characterization
- Water contact angle measurement
- Water swelling ratio measurement
- Synthesis of CM-chitosan-MA
- Anionic functional groups grafted PDMS surface
- Amino acid composition analysis
- Free carboxylic acid and amine contents in ADS
- Clotting assay
- Animal experiments
- *In vivo* biocompatibility and biodegradability evaluation of ADS hydrogel
- *In vivo* application of ADS hydrogel in a rat liver injury model
- *In vivo* application of ADS hydrogel in a rat heart injury model
- Histology and immunohistology
- Statistical analysis

SUPPLEMENTAL INFORMATION

Supplemental information can be found online at https://doi.org/10.1016/j.isci.2022.105106.

ACKNOWLEDGMENTS

WH thanks the National Key Research and Development Program (No. 2021YFA0805904). CZ thanks the support of the National Science Fund for Distinguished Young Scholars (No. 31625011), National Key Research and Development Program (No. 2016YFC1101100), and the Key projects of the National Natural Science Foundation of China (81830055). MX and KM would like to thank NSERC Discovery grants and NSERC Discovery Accelerator Supplements (DAS) Awards for supporting this work.

AUTHOR CONTRIBUTIONS

M.X., H.W., and C.Z. developed the idea and supervised the research project; Y. Liu designed and performed wet adhesion and mechanism related experiments, interpreted data and mechanism, Y. Li designed and conducted *in vivo* experiments; Y. Liu and Y. Li drafted the manuscript; H.S. conducted amino acid composition and protein analysis, analyzed data, and co-wrote the manuscript; W.Z. designed self-adhesion experiments, discussed the mechanism, and revised the paper; Q.W., B.L., and K.M. provided direction on experimental design, discussed the results, and revised the manuscript. All authors commented on the article.

DECLARATION OF INTERESTS

The authors declare no competing interests.

Received: April 20, 2022
Revised: June 23, 2022
Accepted: September 7, 2022
Published: October 21, 2022

REFERENCES

Annabi, N., Zhang, Y.N., Assmann, A., Sani, E.S., Cheng, G., Lassaletta, A.D., Vegh, A., Dehghani, B., Ruiz-Esparza, G.U., Wang, X., et al. (2017). Engineering a highly elastic human protein-based sealant for surgical applications. Sci. Transl. Med. *9*, eaai7466.

Avery, R.K., Albadawi, H., Akbari, M., Zhang, Y.S., Duggan, M.J., Sahani, D.V., Olsen, B.D., Khademhosseini, A., and Oklu, R. (2016). An injectable shear-thinning biomaterial for endovascular embolization. Sci. Transl. Med. *8*, 365ra156. https://doi.org/10.1126/scitranslmed.aah5533.

Baik, S., Kim, D.W., Park, Y., Lee, T.-J., Ho Bhang, S., and Pang, C. (2017). A wet-tolerant adhesive patch inspired by protuberances in suction cups of octopi. Nature *546*, 396–400. https://doi.org/10.1038/nature22382.

Barton, A.F.M. (2017). CRC Handbook of Solubility Parameters and Other Cohesion Parameters, Second edition (CRC Press).

Bouten, P.J., Zonjee, M., Bender, J., Yauw, S.T., van Goor, H., van Hest, J.C., and Hoogenboom, R. (2014). The chemistry of tissue adhesive materials. Prog. Polym. Sci. *39*, 1375–1405. https://doi.org/10.1016/j.progpolymsci.2014.02.001.

Chen, X.-G., and Park, H.-J. (2003). Chemical characteristics of O-carboxymethyl chitosans related to the preparation conditions. Carbohydr. Polym. *53*, 355–359. https://doi.org/10.1016/S0144-8617(03)00051-1.

Chen, X., Yuk, H., Wu, J., Nabzdyk, C.S., and Zhao, X. (2020a). Instant tough bioadhesive with triggerable benign detachment. Proc. Natl. Acad. Sci. USA *117*, 15497–15503. https://doi.org/10.1073/pnas.2006389117.

Chen, Y., Meng, J., Gu, Z., Wan, X., Jiang, L., and Wang, S. (2020b). Bioinspired multiscale wet adhesive surfaces: structures and controlled adhesion. Adv. Funct. Mater. *30*, 1905287. https://doi.org/10.1002/adfm.201905287.

Cui, C., Fan, C., Wu, Y., Xiao, M., Wu, T., Zhang, D., Chen, X., Liu, B., Xu, Z., Qu, B., and Liu, W. (2019). Water-triggered hyperbranched polymer universal adhesives: from strong underwater adhesion to rapid sealing hemostasis. Adv.

Mater. *31*, 1905761. https://doi.org/10.1002/adma.201905761.

Cui, C., and Liu, W. (2021). Recent advances in wet adhesives: adhesion mechanism, design principle and applications. Prog. Polym. Sci. *116*, 101388. https://doi.org/10.1016/j.progpolymsci.2021.101388.

Dang, R., Chen, L., Sefat, F., Li, X., Liu, S., Yuan, X., Ning, X., Zhang, Y.S., Ji, P., and Zhang, X. (2022). A natural hydrogel with prohealing properties enhances tendon regeneration. Small, e2105255. https://doi.org/10.1002/smll.202105255.

Deng, J., Tang, Y., Zhang, Q., Wang, C., Liao, M., Ji, P., Song, J., Luo, G., Chen, L., Ran, X., et al. (2019). A bioinspired medical adhesive derived from skin secretion of Andrias davidianus for wound healing. Adv. Funct. Mater. *29*, 1809110. https://doi.org/10.1002/adfm.201809110.

Dompé, M., Cedano-Serrano, F.J., Heckert, O., van den Heuvel, N., van der Gucht, J., Tran, Y., Hourdet, D., Creton, C., and Kamperman, M. (2019). Thermoresponsive complex coacervate-based underwater adhesive. Adv. Mater. *31*, 1808179. https://doi.org/10.1002/adma.201808179.

Elefteriades, J.A. (2009). How I do it: utilization of high-pressure sealants in aortic reconstruction. J. Cardiothorac. Surg. *4*, 27. https://doi.org/10.1186/1749-8090-4-27.

Feiner, R., Engel, L., Fleischer, S., Malki, M., Gal, I., Shapira, A., Shacham-Diamand, Y., and Dvir, T. (2016). Engineered hybrid cardiac patches with multifunctional electronics for online monitoring and regulation of tissue function. Nat. Mater. *15*, 679–685. https://doi.org/10.1038/nmat4590. https://www.nature.com/articles/nmat4590#supplementary-information.

Gaharwar, A.K., Avery, R.K., Assmann, A., Paul, A., McKinley, G.H., Khademhosseini, A., and Olsen, B.D. (2014). Shear-Thinning nanocomposite hydrogels for the treatment of hemorrhage. ACS Nano *8*, 9833–9842. https://doi.org/10.1021/nn503719n.

Gao, K.-Q., and Shubin, N.H. (2003). Earliest known crown-group salamanders. Nature *422*, 424–428.

Gao, Y., Chen, J., Han, X., Pan, Y., Wang, P., Wang, T., and Lu, T. (2020). A universal strategy for tough adhesion of wet soft material. Adv. Funct. Mater. *30*, 2003207. https://doi.org/10.1002/adfm.202003207.

Gao, Y., Han, X., Chen, J., Pan, Y., Yang, M., Lu, L., Yang, J., Suo, Z., and Lu, T. (2021). Hydrogel–mesh composite for wound closure. Proc. Natl. Acad. Sci. USA *118*. e2103457118. https://doi.org/10.1073/pnas.2103457118.

Geng, X., Wei, H., Shang, H., Zhou, M., Chen, B., Zhang, F., Zang, X., Li, P., Sun, J., Che, J., et al. (2015). Proteomic analysis of the skin of Chinese giant salamander (Andrias davidianus). J. Proteomics *119*, 196–208. https://doi.org/10.1016/j.jprot.2015.02.008.

Guo, W., Ao, M., Li, W., Wang, J., and Yu, L. (2012). Major biological activities of the skin secretion of the Chinese giant salamander, Andrias davidianus. Z. Naturforsch. C J. Biosci. 86–92. https://doi.org/10.1515/znc-2012-1-211.

Guo, Y., Wang, Y., Zhao, X., Li, X., Wang, Q., Zhong, W., Mequanint, K., Zhan, R., Xing, M., and Luo, G. (2021). Snake extract–laden hemostatic bioadhesive gel cross-linked by visible light. Sci. Adv. *7*, eabf9635. https://doi.org/10.1126/sciadv.abf9635.

Han, L., Wang, M., Prieto-López, L.O., Deng, X., and Cui, J. (2020). Self-hydrophobization in a dynamic hydrogel for creating nonspecific repeatable underwater adhesion. Adv. Funct. Mater. *30*, 1907064. https://doi.org/10.1002/adfm.201907064.

Hansen, C.M. (2007). Hansen Solubility Parameters: A User's Handbook, Second Edition (CRC Press).

He, D., Zhu, W., Zeng, W., Lin, J., Ji, Y., Wang, Y., Zhang, C., Lu, Y., Zhao, D., Su, N., and Xing, X.-H. (2018). Nutritional and medicinal characteristics of Chinese giant salamander (Andrias davidianus) for applications in healthcare industry by artificial cultivation: a review. Food Sci. Hum. Wellness *7*, 1–10. https://doi.org/10.1016/j.fshw.2018.03.001.

Hofman, A.H., van Hees, I.A., Yang, J., and Kamperman, M. (2018). Bioinspired underwater adhesives by using the supramolecular toolbox. Adv. Mater. *30*, 1704640. https://doi.org/10.1002/adma.201704640.

Hou, J., Zhu, B., Tong, Y., Li, P., Liu, H., and Wang, X. (2004). Research advances of Chinese giant salamander, Andrias davidianus. Si Chuan Dong Wu *23*, 262–266.

Israelachvili, J., and Wennerström, H. (1996). Role of hydration and water structure in biological and colloidal interactions. Nature *379*, 219–225. https://doi.org/10.1038/379219a0.

Jackson, M., and Mantsch, H.H. (1995). The use and misuse of FTIR spectroscopy in the determination of protein structure. Crit. Rev. Biochem. Mol. Biol. *30*, 95–120. https://doi.org/10.3109/10409239509085140.

Kyte, J., and Doolittle, R.F. (1982). A simple method for displaying the hydropathic character of a protein. J. Mol. Biol. *157*, 105–132. https://doi.org/10.1016/0022-2836(82)90515-0.

Lee, D.W., Lim, C., Israelachvili, J.N., and Hwang, D.S. (2013). Strong adhesion and cohesion of chitosan in aqueous solutions. Langmuir *29*, 14222–14229. https://doi.org/10.1021/la403124u.

Lee, H., Dellatore, S.M., Miller, W.M., and Messersmith, P.B. (2007a). Mussel-inspired surface chemistry for multifunctional coatings. Science *318*, 426–430. https://doi.org/10.1126/science.1147241.

Lee, H., Lee, B.P., and Messersmith, P.B. (2007b). A reversible wet/dry adhesive inspired by mussels and geckos. Nature *448*, 338–341. https://doi.org/10.1038/nature05968.

Li, J., Celiz, A.D., Yang, J., Yang, Q., Wamala, I., Whyte, W., Seo, B.R., Vasilyev, N.V., Vlassak, J.J., Suo, Z., and Mooney, D.J. (2017). Tough adhesives for diverse wet surfaces. Science *357*, 378–381. https://doi.org/10.1126/science.aah6362.

Liu, Y., Xu, K., Chang, Q., Darabi, M.A., Lin, B., Zhong, W., and Xing, M. (2016). Highly flexible and resilient elastin hybrid cryogels with shape memory, injectability, conductivity, and magnetic responsive properties. Adv. Mater. *28*, 7758–7767. https://doi.org/10.1002/adma.201601066.

Liu, X., Zhang, Q., Duan, L., and Gao, G. (2019a). Bioinspired nucleobase-driven nonswellable adhesive and tough gel with excellent underwater adhesion. ACS Appl. Mater. Interfaces *11*, 6644–6651. https://doi.org/10.1021/acsami.8b21686.

Liu, X., Zhang, Q., Duan, L., and Gao, G. (2019b). Tough adhesion of nucleobase-tackifed gels in diverse solvents. Adv. Funct. Mater. *29*, 1900450. https://doi.org/10.1002/adfm.201900450.

Liu, X., Mao, X., Ye, G., Wang, M., Xue, K., Zhang, Y., Zhang, H., Ning, X., Zhao, M., Song, J., et al. (2022a). Bioinspired Andrias davidianus-Derived wound dressings for localized drug-elution. Bioact. Mater. *15*, 482–494. https://doi.org/10.1016/j.bioactmat.2021.11.030.

Liu, Y., Guan, G., Li, Y., Tan, J., Cheng, P., Yang, M., Li, B., Wang, Q., Zhong, W., Mequanint, K., et al. (2022b). Gelation of highly entangled hydrophobic macromolecular fluid for ultrastrong underwater in situ fast tissue adhesion. Sci. Adv. *8*, eabm9744. https://doi.org/10.1126/sciadv.abm9744.

Ma, Y., Hua, M., Wu, S., Du, Y., Pei, X., Zhu, X., Zhou, F., and He, X. (2020). Bioinspired high-power-density strong contractile hydrogel by programmable elastic recoil. Sci. Adv. *6*, eabd2520. https://doi.org/10.1126/sciadv.abd2520.

Mahdavi, A., Ferreira, L., Sundback, C., Nichol, J.W., Chan, E.P., Carter, D.J.D., Bettinger, C.J., Patanavanich, S., Chignozha, L., Ben-Joseph, E., et al. (2008). A biodegradable and biocompatible gecko-inspired tissue adhesive. Proc. Natl. Acad. Sci. USA *105*, 2307–2312. https://doi.org/10.1073/pnas.0712117105.

Mao, X., Yuk, H., and Zhao, X. (2020). Hydration and swelling of dry polymers for wet adhesion. J. Mech. Phys. Solid. *137*, 103863. https://doi.org/10.1016/j.jmps.2020.103863.

Mehdizadeh, M., and Yang, J. (2013). Design strategies and applications of tissue bioadhesives. Macromol. Biosci. *13*, 271–288. https://doi.org/10.1002/mabi.201200332.

Mirfakhrai, T., Madden, J.D., and Baughman, R.H. (2007). Polymer artificial muscles. Mater. Today *10*, 30–38. https://doi.org/10.1016/S1369-7021(07)70048-2.

Murphy, R.W., Fu, J., Upton, D.E., De Lema, T., and Zhao, E.-M. (2000). Genetic variability among endangered Chinese giant salamanders, Andrias davidianus. Mol. Ecol. *9*, 1539–1547. https://doi.org/10.1046/j.1365-294x.2000.01036.x.

Oliveira, N.M., Zhang, Y.S., Ju, J., Chen, A.-Z., Chen, Y., Sonkusale, S.R., Dokmeci, M.R., Reis, R.L., Mano, J.F., and Khademhosseini, A. (2016). Hydrophobic hydrogels: toward construction of floating (Bio)microdevices. Chem. Mater. *28*, 3641–3648. https://doi.org/10.1021/acs.chemmater.5b04445.

Puertas-Bartolomé, M., Benito-Garzón, L., Fung, S., Kohn, J., Vázquez-Lasa, B., and San Román, J. (2019). Bioadhesive functional hydrogels: controlled release of catechol species with

antioxidant and antiinflammatory behavior. Mater. Sci. Eng. C Mater. Biol. Appl. *105*, 110040. https://doi.org/10.1016/j.msec.2019.110040.

Rose, S., Prevoteau, A., Elzière, P., Hourdet, D., Marcellan, A., and Leibler, L. (2014). Nanoparticle solutions as adhesives for gels and biological tissues. Nature *505*, 382–385. https://doi.org/10.1038/nature12806.

Sani, E.S., Kheirkhah, A., Rana, D., Sun, Z., Foulsham, W., Sheikhi, A., Khademhosseini, A., Dana, R., and Annabi, N. (2019). Sutureless repair of corneal injuries using naturally derived bioadhesive hydrogels. Sci. Adv. *5*, eaav1281. https://doi.org/10.1126/sciadv.aav1281.

Sharma, B., Fermanian, S., Gibson, M., Unterman, S., Herzka, D.A., Cascio, B., Coburn, J., Hui, A.Y., Marcus, N., Gold, G.E., and Elisseeff, J.H. (2013). Human cartilage repair with a photoreactive adhesive-hydrogel composite. Sci. Transl. Med. *5*, 167ra6. https://doi.org/10.1126/scitranslmed.3004838.

Spotnitz, W.D. (2010). Fibrin sealant: past, present, and future: a brief review. World J. Surg. *34*, 632–634. https://doi.org/10.1007/s00268-009-0252-7.

Steck, J., Kim, J., Yang, J., Hassan, S., and Suo, Z. (2020). Topological adhesion. I. Rapid and strong topohesives. Extreme Mech. Lett. *39*, 100803. https://doi.org/10.1016/j.eml.2020.100803.

Su, Q., Wei, D., Dai, W., Zhang, Y., and Xia, Z. (2019). Designing a castor oil-based polyurethane as bioadhesive. Colloids Surf. B Biointerfaces *181*, 740–748. https://doi.org/10.1016/j.colsurfb.2019.06.032.

Tiu, B.D.B., Delparastan, P., Ney, M.R., Gerst, M., and Messersmith, P.B. (2020). Cooperativity of catechols and amines in high-performance dry/wet adhesives. Angew. Chem. Int. Ed. Engl. *59*, 16616–16624. https://doi.org/10.1002/anie.202005946.

Trott, A.T. (1997). Cyanoacrylate tissue adhesives: an advance in wound care. JAMA *277*, 1559–1560. https://doi.org/10.1001/jama.1997.03540430071037.

Wang, L., Liu, Y., Ye, G., He, Y., Li, B., Guan, Y., Gong, B., Mequanint, K., Xing, M.M.Q., and Qiu, X. (2021). Injectable and conductive cardiac patches repair infarcted myocardium in rats and minipigs. Nat. Biomed. Eng. *5*, 1157–1173. https://doi.org/10.1038/s41551-021-00796-9.

Wang, L.-F., Li, X.-Y., and Wang, D.-Z. (2011). Characterization and bioactivity of antimicrobial peptides from the skin secretions of the Andrias davidianus. Chin. J. Biochem. Pharm. *32*, 269–272.

Wu, S.J., Yuk, H., Wu, J., Nabzdyk, C.S., and Zhao, X. (2021). A multifunctional origami patch for minimally invasive tissue sealing. Adv. Mater. 2007667. https://doi.org/10.1002/adma.202007667.

Xi, C., Yang-ke, W., and De-jing, C. (2012). The pharmacological research of cure burn by the ointment of giant salamander's skin and mucus hubei. Agric. Sci. *13*, 042.

Xu, K., Liu, Y., Bu, S., Wu, T., Chang, Q., Singh, G., Cao, X., Deng, C., Li, B., Luo, G., and Xing, M. (2017). Egg albumen as a fast and strong medical adhesive glue. Adv. Healthc. Mater. *6*, 1700132. https://doi.org/10.1002/adhm.201700132.

Yang, J., Bai, R., and Suo, Z. (2018). Topological adhesion of wet materials. Adv. Mater. *30*, 1800671. https://doi.org/10.1002/adma.201800671.

Yuk, H., Varela, C.E., Nabzdyk, C.S., Mao, X., Padera, R.F., Roche, E.T., and Zhao, X. (2019). Dry double-sided tape for adhesion of wet tissues and devices. Nature *575*, 169–174. https://doi.org/10.1038/s41586-019-1710-5.

Zhang, W., Wang, R., Sun, Z., Zhu, X., Zhao, Q., Zhang, T., Cholewinski, A., Yang, F.K., Zhao, B., Pinnaratip, R., et al. (2020). Catechol-functionalized hydrogels: biomimetic design, adhesion mechanism, and biomedical applications. Chem. Soc. Rev. *49*, 433–464. https://doi.org/10.1039/c9cs00285e.

Zhang, X., Jiang, L., Li, X., Zheng, L., Dang, R., Liu, X., Wang, X., Chen, L., Zhang, Y.S., Zhang, J., and Yang, D. (2022). A bioinspired hemostatic powder derived from the skin secretion of Andrias davidianus for rapid hemostasis and intraoral wound healing. Small *18*, 2101699. https://doi.org/10.1002/smll.202101699.

Zhao, Q., Lee, D.W., Ahn, B.K., Seo, S., Kaufman, Y., Israelachvili Jacob, N., and Waite, J.H. (2016). Underwater contact adhesion and microarchitecture in polyelectrolyte complexes actuated by solvent exchange. Nat. Mater. *15*, 407. https://doi.org/10.1038/nmat4539.

STAR★METHODS

KEY RESOURCES TABLE

REAGENT or RESOURCE	SOURCE	IDENTIFIER
Biological samples		
Andrias Davidianus secretion (ADS)	In-house collected skin secretion from adult Andrias Davidianus (Sichuan China)	N/A
Porcine skin tissue	Local meat store (Manitoba Canada)	N/A
Anti-CD68 antibody	Abcam	Abcam Cat# ab283654; RRID:AB_2922954
Anti-CD3 antibody	Abcam	Abcam Cat# ab16669; RRID:AB_443425
Alexa Fluor 568-conjugated secondary antibodies	Abcam	Abcam Cat# ab175471, RRID:AB_2576207
DAPI	Abcam	ab228549
Sprague Dawley (SD) rats, 6-week-old	The Animal Experimental Center of Third Military Medical University	N/A
Chemicals, peptides, and recombinant proteins		
α-Cyanoacrylate adhesives	Guangzhou Baiyun Medical Adhesive Co., Ltd., Guangzhou, China	N/A
Porcine Fibrin Sealant Kit	Hangzhou Puji Medicine Technology Development Co.Ltd, Hangzhou, China	N/A
SYLGARD®184 silicone elastomer kit	Dow corning Company	SYLGARD®184
Hexafluoroisopropanol	Synquest Laboratories	2102-3-X6
Chitosan (low viscosity: < 200mPa•s)	Aladdin	C105801
Sodium hydroxide	Sigma Aldrich	S5881
Acetic acid	Sigma Aldrich	A6283
Alginic acid sodium salt, low viscosity	Alfa Aesar	B25266
Methacrylic anhydride	Sigma Aldrich	276685
(3-aminopropyl) trimethoxysilane	Sigma Aldrich	281778
N-Hydroxysuccinimide	Sigma Aldrich	130672
N-(3-Dimethylaminopropyl)-*N*′-ethylcarbodiimide hydrochloride	Sigma Aldrich	E7750
Hydrochloric acid	Sigma Aldrich	320331
Isoflurane	Shenzhen RWD Life Science Co., Ltd. , China	R510-22
4% paraformaldehyde	Beyotime (Shanghai, China)	P0099-100mL
Software and algorithms		
ImageJ	ImageJ	https://imagej.nih.gov/ij/
GraphPad Prism 8	GraphPad	https://www.graphpad.com/

RESOURCE AVAILABILITY

Lead contact

Further information and requests should be directed to the lead contact: Wei Hong, Malcolm Xing, and Chuhong Zhu.

Materials availability

All data are available in the main manuscript and supplementary information. This study does not generate new unique reagents.

Data and code availability

All data produced in this study are included in the published article and its supplementary information.

This study does not report original code.

EXPERIMENTAL MODEL AND SUBJECT DETAILS

In vivo biocompatibility and biodegradability evaluation of ADS hydrogel

Male Sprague Dawley rats (200–250g) were anesthetized with 1–1.5% isoflurane. After the creation of skin incisions (about 1.5 cm long) on the dorsum of the rat, the subcutaneous pockets were implanted with ADS hydrogels and then closed by suturing. At day 7, 14, and 28, the animals were euthanized by CO_2 inhalation.

In vivo application of ADS hydrogel in a rat liver injury model

Male Sprague Dawley rats (200–250g) were anesthetized with 1–1.5% isoflurane. After the abdomen was open, a severe laceration of 2–3 cm long on the lobe of rat's liver was created with a scalpel.

In vivo application of ADS hydrogel in a rat heart injury model

Male Sprague Dawley rats (200–250g) were anesthetized with 1–1.5% isoflurane. Breathing was maintained by a ventilator. After a left lateral thoracotomy, the ventriculus sinister of the rat heart was exposed and then punctured by a needle of 1 mm diameter. ADS powder was applied onto the lesion site and pressed to stop bleeding immediately. The chest incisions were closed with sutures, and rats were returned to their cages after recovery from anesthesia.

METHOD DETAILS

Andrias davidianus secretion (ADS)

ADS powder was harvested from Chinese giant salamander skin, lyophilized and then ground to fine powder, and finally stored at 4°C before use. Porcine skin tissues were from a local market and frozen at −20°C till use. Before use, the fat tissue on porcine skin was removed with a knife, and the cleaned porcine skin was soaked in water and stored at 4°C. Cyanoacrylate adhesives were purchased from Guangzhou Baiyun Medical Adhesive Co., Ltd. Porcine fibrin sealant was purchased from Hangzhou Puji Medicine Technology Development Co. Ltd. SYLGARD®184 silicone elastomer and the corresponding curing agent were obtained from Dow Corning Corporation. Hexafluoroisopropanol (HFIP) was purchased from SynQuest Laboratories. Chitosan (low viscosity: < 200mPa•s) was purchased from Aladdin. All other chemicals used in the experiments were purchased from Sigma-Aldrich and used directly without further purification.

Lap shear adhesion test

A universal tensile tester (Instron 5965) was employed to determine the lap shear adhesion of different adhesives on diverse substrates. The PDMS substrate was prepared by curing SYLGARD®184 silicone elastomer at 80°C, and cut to a rectangular shape with a width of 10 mm. Porcine skin tissue was freshly prepared by thawing the stored bulk product at room temperature for1h and then cut into the rectangular shape with a width of 10mm. For cyanoacrylate or fibrin glue adhesive, ∼50μL adhesive or mixture was cast on one end of the rectangular substrate (in a region of 10mm × 10mm), which was then covered by another piece of the substrate. The adhered substrate was cured for 5 min under an external weight of 500g before the test. For ADS, a region of 10mm × 10 mm of the substrate was covered by a layer of ADS fine powder (∼25mg), and then 25μL of water was dropped onto ADS powder, which was sequentially sandwiched by another piece of substrate. The adhered substrate was cured under the same condition described above. The lap shear adhesion was measured on a universal tester (Instron 5965) equipped with a loading cell of 500N at a tensile rate of 5 mm/min for all samples. Underwater shear adhesion tests were conducted similarly while fully soaked in water for different times before the test and were measured instantly once taken out of water.

Cohesive energy of ADS the granular hydrogel with different swelling ratios

Cohesive energy was measured by cyclic tensile test using INSTRON 5965. The ADS hydrogel patch was prepared by sandwiching ADS and water mixture between 2 glass slides. Typically, 150 mg ADS powder was sandwiched with 2 glass slides to form a uniform layer, and the top glass slide was removed. Then, 150l, 300l or 450μL of water was dispensed on the ADS layer, which was covered by the top glass slide again

for 30 s to prepare ADS hydrogel with different water content. The ADS hydrogel sample with maximum swelling ratio was further soaked in water for 3 h to achieve maximum swelling. The formed ADS hydrogel patch had a uniform shape to prevent the formation of any cracks. The patch was then challenged with a cyclic tensile deformation of 150% strain for 1 cycle. The cohesive (dissipated) energy was calculated by integrating the area of the formed cycle in the stress-strain curve.

SEM characterization

The SEM characterization of the hydrogel morphology was performed on a JEOL-5900 scanning electron microscope. The samples with their substrates were lyophilized together, and then the sample-substrate interface part and internal cross-section area were selected and sputter-coated with a thin layer of gold for characterization.

FTIR identification of ADS secondary structure fractions

The secondary structure fractions of dry ADS powder or ADS granular hydrogel with different water swelling ratio was quantified by FTIR-ATR spectra, performed on a Nicolet iS10 FTIR Spectrometer with a scan number of 32 and resolution of 4. The protein secondary structures of ADS were quantified by analyzing its FTIR-FTR spectrum peaks in the amide I region. The raw curve of FTIR spectrum was self-deconvoluted to overlain single peaks, which were fitted by Gaussian fitting to obtain all single peaks and their peak areas (all fitted peaks were in accordance with the corresponding secondary derivative trace). Therefore, the secondary structure fractions were calculated according to the corresponding peak areas.

Rheological characterization

All rheology experiments were performed on TA Discovery Hybrid Rheometer at the temperature of 25°C. The normal stress of adhesives was measured on steel parallel plates with 8 mm diameter geometry. After the adhesive was sandwiched and held between two plates under a normal force of 0.5N to cure for 5 min, the supper plate moved along the axial direction at the rate of 1 μm/s. For cyanoacrylate and fibrin glue, 50μL of adhesive was applied each test, and 25mg powder with 25μL of water was applied for ADS.

The rheological measurements of 5% ADS-acetic acid solution, 1% alginate sodium solution and ADS-alginate mixture were conducted on a cone and plate with a geometry of 20mm diameter and 2° cone angle. The frequency was ramped from 0.1 rad/s to 100 rad/s with a constant strain of 0.5%.

The storage module (G′) and loss module (G″) of the hydrogel and self-adhered hydrogel were determined by frequency sweeping from 0.1 rad/s to 100 rad/s with a constant strain of 1.0% under parallel plates with 8 mm diameter. The time sweeping rheology test with alternating amplitudes was run on self-adhered ADS hydrogel. The amplitudes of 0.1% or 100% strains were alternated at the interval of 200 s under a constant shear rate of 1 rad/s for 8 steps.

Wet adhesion behavior of self-assembled ADS hydrogel

The dry ADS particulates (~100mg) and a cotton thread bound to a 50-gram weight were sandwiched by two glass slides and placed in a glass petri dish. 50 mL of water was poured into the petri dish and then sandwiched ADS particulates were soaked in water for ~20s for self-assembly. Then the sandwiched ADS patches with glass slides were lifted out of the water surface, which could hold a weight of 50 g successfully through the adhered cotton thread. One glass slide of the sandwich structure was carefully removed with a razor blade, and therefore the ADS hydrogel patch was only adhered to one glass slide and fully contacted with water. The glass slide with ADS patch was hanged on the wall of the glass beaker and soaked in water, which still held the weight standard of 50g through the cotton thread. The ADS hydrogel patch was still adhered to the glass slide after 7 days.

Optical microscope characterization

The real-time observation of ADS granular self-assembly was conducted on optical microscopy (Saike Digital) equipped with a camera (Samsung) at the magnification of 40X. ADS particulates were dispersed on a glass slide and covered by a thin coverslip, and water droplets were dropped to one side of the coverslip and spread to contact the ADS particulates. The particle size and size distribution were measured by optical microscope photograph and quantified using Image J software.

Water contact angle measurement

An optical contact angle measurement instrument (JY-PHA, SINDIN company) was used for water contact angle measurements and real-time video recording of water droplets contacting ADS powder. The ADS hydrogel patches used for water contact angle measurements were prepared as described above, and the water swelling ratio was 100%. 5 μL water droplets were used for measurement.

Water swelling ratio measurement

The ADS hydrogel patch was prepared according to the protocol described above, and ADS hydrogel patches containing 100% water were prepared for swelling ratio measurement. The swelling ratio was evaluated by the weight change of ADS patches soaked in water up to 6 h. The patches were taken out of the water to weigh at different time points, and all water on surface should be cleaned before weighing. The water swelling ratio can be calculated as follow:

$$\text{Swelling ratio} = \left(W_{overall} - W_{dry}\right)/W_{dry} \times 100\%$$

where $W_{overall}$ is the overall weight of ADS hydrogel at time point t, W_{dry} is the weight of dry ADS powder.

Synthesis of CM-chitosan-MA

Methacrylated Carboxymethyl chitosan (CM-chitosan-MA) was prepared as a model compound to mimic the adhesion and underwater adhesion behavior of ADS. Carboxymethylation of chitosan was prepared in accordance with previously published literature (Chen and Park, 2003). Briefly, 2 g of chitosan and 2.7 g of NaOH were dispersed in the 20 mL mixture of isopropyl alcohol and water (volume ratio 9:1). The mixture was stirred and alkalized in an oil bath of 50°C for 1 h, and then 4 mL isopropyl alcohol solution of monochloroacetic acid (3 g) was dropped into the mixture and heated for another 4h with stirring at 50°C. The reaction was terminated by cooling down, and the product was precipitated out of 70% aqueous ethanol solution. The obtained product was dissolved in water and dialyzed against DI water in dialysis tubing with an MWCO of 8000–14000 Da for 2 days. Carboxymethyl chitosan (CM-chitosan) was obtained after lyophilization.

Methacrylate groups were introduced onto CM-chitosan backbone by reacting with methacrylic anhydride. In a typical reaction, 1g CM-chitosan was dissolved in 50mL of DI water at 50°C, and then cooled down to room temperature. 1 mL of methacrylic anhydride was dropped into the solution slowly, and the mixture was stirred at room temperature for 20 h. After the reaction, the solution was transferred to a dialysis tubing (MWCO = 8000–14000 Da) against DI water for 3days. Finally, CM-chitosan-MA was recovered from lyophilization and was ground to a fine powder with liquid nitrogen as a self-assembled adhesive. FTIR-ATR and ^{1}H NMR were employed to characterize the chemical structures of CM-chitosan and CM-chitosan-MA.

Anionic functional groups grafted PDMS surface

Considering the presence of negative charges on the human tissue surface, we modified the soft PDMS substrate surface with polyacrylic acids to obtain a soft substrate with a negatively charged surface. The SYLGARD®184 PDMS thin sheet was prepared in advance through mixing base and catalyst at the ratio of 10:1, removing bubbles and thermally curing at 80°C according to the instruction. The PDMS sheets were treated with hot piranha (30% H_2O_2: concentrated H_2SO_4 = 2:3) for 30 min to introduce more hydroxyl groups onto the surface. After treatment, the sheets were soaked in 1M KOH solution for another 30 min, and then repeatedly rinsed with DI water. After rinsing with DI water, hydrophilic-modified PDMS surface was sequentially decorated with primary amines by silanization of (3-aminopropyl) trimethoxysilane (AMPTMS). PDMS sheets were immersed in the DMF solution of AMPTMS (2mL of AMPTMS +20mL DMF and 0.6 mL DI water) at 65°C for 15 h. After the reaction, the samples were washed with DI water completely to remove unreacted silanes. Finally, poly (acrylic acid) (PAA, Mw: ~60000 Da, sodium salt form, protonated by HCl) was grafted onto PDMS through amidation catalyzed with EDC/NHS. PAA sodium salt was protonated with 0.1M HCl a.q. solution in advance, and then PDMS sheets were soaked in 20mL PAA a.q. solution for 24 h in the presence of EDC/NHS catalyst. After the reaction, PDMS sheets were rinsed with DI water completely and dried in air. The PAA conjugated PDMS sheets were used as anionic charges containing PDMS substrate.

Amino acid composition analysis

The amino acid composition quantification was carried out on Hitachi Amino Acid Analyzer L-8900. ADS sample was grounded and filtered through a filter screen of 60 mesh before the test. 300mg of ADS powder

was weighed into a 20 mLAmpere bottle, and then 10 mL of HCl aqueous solution (6.0 mol/L) was added. The mixture was frozen in liquid nitrogen, vacuumed to less than 7 Pa, and then sealed. The container was placed in an oven at 110 ± 1°C for hydrolyzing the proteins. After hydrolysis of 22–24h, the mixture was cooled down and filtered. Contain amount of aliquot of solution was collected and dried by rotational evaporation. A small amount of water was added to re-dissolve the product, and then dried again by rotational evaporation. This procedure was repeated once or twice. The dry product was dissolved in 3∼5mL dilute HCl (0.02 mol/L, pH 2.2) for the test, and the concentration of amino acids in the sample solution should be ∼100 nmol/mL. The sample solution was mixed well and centrifuged, and the supernatant was used for quantification.

According to instrument instruction, a standard working solution of amino acids was prepared at the concentration of 2 nmol/20μL, and sodium citric acid buffer with different pH value was used as eluent. The hydrolyzed sample solution and mixed corresponding amino acid working standard solution were sequentially injected for quantification analysis. The mass of amino acids (mg) per kg sample could be calculated according to the following equation:

$$X = \frac{m1}{m} \times n$$

where, X = the mass of amino acids per kg sample (mg); m1: the amount of amino acids of corresponding peaks on sample chromatographic spectrum (μg); m: sample weight (g); n: dilution factor.

Free carboxylic acid and amine contents in ADS

Thefree amine group content in ADS was determined by potentiometric titration and 0.68% free amine groups were measured. The free carboxylic acid group content was confirmed by titration with dilute sodium hydroxide solution and 0.95% free carboxylic acids were measured.

Clotting assay

Citrated whole blood (containing 0.109 M sodium citrate) was mixed with 10% (v/v) $CaCl_2$ (0.1M) to prepare standard blood sample for cloting assay. 50 μL per well was pipetted into sequential wells on a 96-well plate. Then, saline solution (0.9%) was added into corresponding well at each time point to terminate the clotting process, and all soluble blood components were removed. For experimental group, the bottom surface of each well was pre-covered with a thin layer of ADS powder (4 mg). Once a uniform size of clot was formed among sequencial wells, the assay can be finished. The time that first formed the uniform size of clot was marked as the clotting time. Clots with ADS hydrogel were fixed overnight with glutaraldehyde, lyophilized, and characterized with SEM (ZEISS Crossbeam 340) to investigate the interaction between ADS and blood components.

Animal experiments

All animal experiments were carried out in accordance with the regulations of ethical approval for research involved animals and were approved by the Ethics Committee of the Third Military Medical University.

In vivo biocompatibility and biodegradability evaluation of ADS hydrogel

Before implantation, the ADS samples were prepared, weighed, and sterilized (60–70 mg). Male Sprague Dawley rats (200–250g) were anesthetized with 1–1.5% isoflurane. After the creation of skin incisions (about 1.5 cm long) on the dorsum of the rat, the subcutaneous pockets were implanted with ADS hydrogels and then closed by suturing. At day 7, 14, and 28, the animals were euthanized by CO_2 inhalation, and the ADS implants with the surrounding tissue were excised for further histological analysis.

In vivo application of ADS hydrogel in a rat liver injury model

Before surgery, male Sprague Dawley rats (200–250g) were anesthetized as described above. After the abdomen was open, a severe laceration of 2–3 cm long on the lobe of rat's liver was created with a scalpel. Then, dry ADS powder (10–20 mg) was applied to the lesion region and immediately pressed with a glass plate. One minute later, with the formation of a free-standing hydrogel layer on the wound site, a brief assessment of the adhesion strength between ADS hydrogel and lesion liver proceeded with tweezers. During the treatment, the blood loss was also carefully collected with a filter paper to quantify the hemostatic efficiency of ADS hydrogel.

In vivo application of ADS hydrogel in a rat heart injury model

The heart sealing capacity of ADS hydrogel was tested on rats. Anesthesia was performed as described previously. Breathing was maintained by a ventilator. After a left lateral thoracotomy, the ventriculus sinister of the rat heart was exposed and then punctured by a needle of 1 mm diameter. ADS powder was applied onto the lesion site and pressed to stop bleeding immediately. The chest incisions were closed with sutures, and rats were returned to their cages after recovery from anesthesia. Four weeks later, the cardiac function of rats was evaluated by echocardiography measurements (Vevo 2100, VisualSonics).

Histology and immunohistology

ADS hydrogel and surrounding tissue were used for histological analysis. Samples with the surrounding tissue were fixed overnight with glutaraldehyde and lyophilized for characterization of ADS-tissue interface with SEM (ZEISS Crossbeam 340). The sections were fixed with 4% paraformaldehyde/PBS at 4°C overnight and then processed for H&E staining. Anti-CD68, anti-CD3 (Abcam), primary antibodies with Alexa Fluor 568–conjugated (Life Technologies) secondary antibodies were applied to immunofluorescence staining. The sections were further stained by DAPI (Abcam). The H&E-stained sections were imaged with a Leica microscope (DM IL LED). The immunofluorescence-stained sections were imaged with a confocal microscope (LSM800, Zeiss).

Statistical analysis

Data are presented as the mean ± SD. Significance was determined using Student's *t*-test. ***$p < 0.001$ was defined as statistically significant. All statistical analysis was performed with the GraphPad Prism version 8 software.